Article

Molecular Cell

VPS34 Acetylation Controls Its Lipid Kinase Activity and the Initiation of Canonical and Non-canonical Autophagy

Graphical Abstract

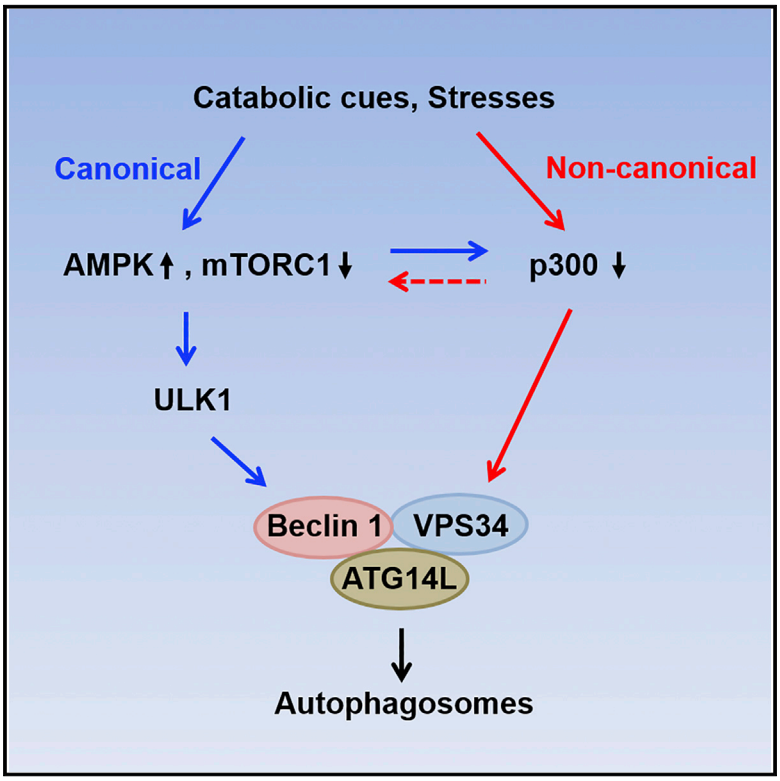

Authors

Hua Su, Fei Yang, Qiuting Wang, ..., Fudi Wang, Tianhua Zhou, Wei Liu

Correspondence

liuwei666@zju.edu.cn

In Brief

Su et al. report a novel mechanism for the activity regulation of lipid kinase VPS34. The acetyltransferase p300-mediated acetylation inhibits VPS34 activity. Deacetylation of VPS34 enhances VPS34-PI interaction and VPS34-Beclin 1 core complex formation. This p300-VPS34 pathway is critical to the initiation of canonical and non-canonical autophagy.

Highlights

- VPS34 is a direct target of acetyltransferase p300
- Deacetylation of VPS34 is required for canonical and non-canonical autophagy
- Acetylation of VPS34 hinders VPS34-PI and VPS34-Beclin 1 interactions
- Acetyltransferase p300 is an alternative homeostatic sensor

Su et al., 2017, Molecular Cell 67, 1–15
September 21, 2017
http://dx.doi.org/10.1016/j.molcel.2017.07.024

CellPress

Please cite this article in press as: Su et al., VPS34 Acetylation Controls Its Lipid Kinase Activity and the Initiation of Canonical and Non-canonical Autophagy, Molecular Cell (2017), http://dx.doi.org/10.1016/j.molcel.2017.07.024

Molecular Cell
Article

VPS34 Acetylation Controls Its Lipid Kinase Activity and the Initiation of Canonical and Non-canonical Autophagy

Hua Su,[1] Fei Yang,[1] Qiuting Wang,[1] Qiuhong Shen,[1] Jingtao Huang,[1] Chao Peng,[3] Yi Zhang,[1] Wei Wan,[1] Catherine C.L. Wong,[3] Qiming Sun,[1] Fudi Wang,[1] Tianhua Zhou,[1] and Wei Liu[1,2,4,*]
[1]Department of Biochemistry and Molecular Biology, Program in Molecular and Cell Biology, Zhejiang University School of Medicine, Hangzhou 310058, China
[2]Collaborative Innovation Center for Diagnosis and Treatment of Infectious Disease, First Affiliated Hospital, Zhejiang University School of Medicine, Hangzhou 310003, China
[3]National Center for Protein Science Shanghai, Institute of Biochemistry and Cell Biology, Shanghai Institutes of Biological Sciences, Chinese Academy of Sciences, Shanghai 200031, China
[4]Lead Contact
*Correspondence: liuwei666@zju.edu.cn
http://dx.doi.org/10.1016/j.molcel.2017.07.024

SUMMARY

The class III phosphoinositide 3-kinase VPS34 plays a key role in the regulation of vesicular trafficking and macroautophagy. So far, we know little about the molecular mechanism of VPS34 activation besides its interaction with regulatory proteins to form complexes. Here, we report that VPS34 is specifically acetylated by the acetyltransferase p300, and p300-mediated acetylation represses VPS34 activity. Acetylation at K771 directly diminishes the affinity of VPS34 for its substrate PI, while acetylation at K29 hinders the VPS34-Beclin 1 core complex formation. Inactivation of p300 induces VPS34 deacetylation, PI3P production, and autophagy, even in *AMPK*$^{-/-}$, *TSC2*$^{-/-}$, or *ULK1*$^{-/-}$ cells. In fasting mice, liver autophagy correlates well with p300 inactivation/VPS34 deacetylation, which facilitates the clearance of lipid droplets in hepatocytes. Thus, p300-dependent VPS34 acetylation/deacetylation is the physiological key to VPS34 activation, which controls the initiation of canonical autophagy and of non-canonical autophagy in which the upstream kinases of VPS34 can be bypassed.

INTRODUCTION

Phosphatidylinositol 3-phosphate (PI3P), one of the most versatile phosphoinositides, is generated from phosphatidylinositol (PI) mainly by VPS34 (vacuolar protein sorting 34), a class III PI3 kinase (PI3KC3). VPS34 is the only PI3KC3 in mammals, and its activation at phagophore and endosomal membranes, in which key proteins with PI3P-binding domains are recruited for membrane remodeling, is pivotal for autophagy and endosomal transport (Backer, 2008). During autophagy, VPS34 interacts with Beclin 1, ATG14L, and p150 at the phagophore to form functional complexes (Matsunaga et al., 2010). It has been suggested that the formation of the Beclin 1-VPS34 core complex is required for VPS34 activation in autophagy and is governed primarily by the serine/threonine kinase ULK1 which phosphorylates Beclin 1 in response to signals from the major homeostatic sensors AMPK and mTORC1 (Russell et al., 2013; Kim et al., 2011).

In addition to the generation of PI3P, which occurs at the phagophore membrane and is controlled mainly by protein phosphorylation, another key step in autophagy induction is the conjugation of LC3 (the microtubule-associated protein 1 light chain 3, a mammalian homolog of yeast Atg8) to phosphatidylethanolamine (PE), which facilitates the membrane binding of LC3, thereby enabling the growth and elongation of autophagic membranes (Ichimura et al., 2000; Kabeya et al., 2004). Recently, emerging evidence has indicated that LC3-PE conjugation is regulated by an intracellular acetylation/deacetylation system that involves a number of Atg proteins and key acetyltransferases/deacetylases (Bánréti et al., 2013; Huang et al., 2015; Lee and Finkel, 2009; Lee et al., 2008). This suggests that autophagy-initiating signals, which in most cases derive from cell homeostatic sensors, need to coordinate the activation of phosphorylation-regulated PI3P production and acetylation-controlled LC3-PE conjugation. A striking example is the activation of AMPK, which in turn activates VPS34 by phosphorylating ULK1 and/or Beclin 1 (Russell et al., 2013; Kim et al., 2011, 2013) and the deacetylase Sirt1 by elevating cellular NAD^+ or mediating the Sirt1-GAPDH interaction (Cantó et al., 2009; Chang et al., 2015). Changes in cellular acetylation status sufficiently trigger autophagy (Mariño et al., 2014; Pietrocola et al., 2015a), thereby suggesting a role of acetyltransferases/deacetylases in PI3P production, in addition to their effect on LC3-PE conjugation. Theoretically, acetyltransferases/deacetylases can exert their effect by targeting upstream kinases (Lin et al., 2012), VPS34 complex components (Sun et al., 2015), or VPS34 itself.

Recently, it has been suggested that non-canonical autophagy leads to lysosomal degradation through variants of the canonical pathway (Codogno et al., 2011). These alternative routes underscore the complexity of the molecular aspects of

autophagy, because many of them involve unconventional biogenesis of canonical autophagosomes, which does not require the proteins that are important for homeostasis sensing (Grotemeier et al., 2010; Lipinski et al., 2010; Cheong et al., 2011; Smith et al., 2010). This suggests that the AMPK-mTORC1-ULK1 circuit can be bypassed for PI3P production and autophagy initiation under certain conditions. However, the mechanisms underlying this phenomenon are unknown.

In this study, we have identified a pivotal role of p300-mediated VPS34 acetylation in controlling VPS34 activity. We show that this mechanism of VPS34 regulation is employed in the initiation not only of canonical autophagy stimulated by cell starvation but also of non-canonical autophagy in which the activation of VPS34 is independent of upstream kinases. Our findings highlight and explain the importance of p300 in the regulation of the early events of autophagy.

RESULTS

VPS34 Is Acetylated by p300 at K29, K771, and K781

Nutrient starvation causes a reduction in cytoplasmic protein acetylation, and this involves suppression of the acetyltransferase p300 (Mariño et al., 2014). Using a web server that predicts protein sites that are specifically acetylated by lysine acetylation transferases (http://bioinfo.bjmu.edu.cn/huac/), we proposed that VPS34 is an acetylated protein and p300 is the responsible acetyltransferase. To verify the proposal, we first set up an assay to detect acetylated VPS34. We treated cells with the broad-spectrum HDAC deacetylase family inhibitor trichostatin A (TSA) and the SIRT deacetylase family inhibitor nicotinamide (NAM). These treatments markedly augmented VPS34 acetylation compared to the basal level in untreated cells (Figure 1A). Acetylation is dependent on the levels of acetyl coenzyme A (acetyl-CoA) in cells. Utilizing in cells a pyruvate dehydrogenase kinase inhibitor dichloroacetate (DCA) or a mitochondrial pyruvate carrier inhibitor α-cyano-β-(1-phenylindol-3-yl)acrylate (UK5099) to increase or decrease intracellular acetyl-CoA (Mariño et al., 2014), we found that VPS34 acetylation was enhanced or suppressed correspondingly (Figures S1A and S1B). We then ectopically expressed each of the most common acetyltransferases and found that only p300 enhanced VPS34 acetylation (Figure 1B). The enhancement was not seen even with CBP (CREB-binding protein), a paralog of p300. This effect was verified by using the specific p300 activator N-(4-chloro-3-trifluoromethyl-phenyl)-2-ethoxy-benzamide (CTB) and the p300 inhibitor C646, I-CBP112, or SGC-CBP30 (Figures 1C and S1C). Further, the basal acetylation of VPS34 was inhibited by p300 RNAi, and this inhibition was reversed by expression of wild-type but not an acetyltransferase-dead p300 (p300-WY, Bordoli et al., 2001) (Figure 1D). These results thus suggest that VPS34 is regulated by p300-mediated acetylation.

We then asked whether VPS34 is a direct p300 substrate, as a number of cytoplasmic proteins can interact with p300 (Sebti et al., 2014; Shi et al., 2009). First we examined the distribution of p300 in the cytosol in our experimental system by cellular fractionation. We found that p300 and its acetylation were detectable in the cytosol fraction (Figure S1D). Intriguingly, SGC-CBP30 treatment abolished the acetylation of both cytosolic and nuclear p300, and meanwhile the acetylation of VPS34 (Figure S1D), suggesting an effect of cytosolic p300 on VPS34 acetylation. We then detected a co-immunoprecipitation of endogenous p300 with endogenous VPS34 from cells which was enhanced by CTB (Figure 1E). Further, we incubated purified recombinant GST-VPS34 with p300-HA immunoprecipitated from cells or with the p300 HAT domain (catalytic domain) purified from *E. coli*. GST-VPS34 was acetylated by both p300-HA and the p300 HAT domain (Figures 1F and 1G), but not the acetyltransferase-dead p300 (Figure 1F), and the acetylation was enhanced by CTB and fully blocked by C646 (Figure 1F). Finally, we cultured GST-VPS34 with p300 immunoprecipitated from the cytosol fraction and confirmed in vitro its sufficient activity on VPS34 (Figure S1E).

Mass spectrometry of the acetylated GST-VPS34 suggested five potential acetylation sites which are located in different domains of VPS34 and are conserved in different species (Figures S1F and S1G). To verify these sites, Flag-tagged VPS34 mutants in which each of the five lysine residues was changed to arginine via site-directed mutagenesis were constructed and transfected into cells. Acetylation assessment affirmed that K29 in the N-terminal C2-domain, and K771 and K781 in the C-terminal catalytic domain, are the major acetylated residues (Figures 1H and 1I). To measure quantitatively the degree of VPS34 acetylation at the identified sites in cells, we immunoprecipitated VPS34 from cells treated with CTB or SGC-CBP30 and assessed the stoichiometry of VPS34 acetylation by spectral counting (Asara et al., 2008). In untreated cells, VPS34 acetylated at the specific sites accounted for ~10% of the total VPS34, when acetylated VPS34 at each of the sites accounted for less than 5% of the total (Figures S1H and S1I). While CTB treatment elevated the acetylations up to 3-fold, SGC-CBP30 dramatically reduced them down to less than 1% (Figures S1H and S1I).

Acetylation by p300 Suppresses VPS34 Lipid Kinase Activity

We then evaluated the impact of VPS34 acetylation on PI3P production. Activating or inactivating p300 in cells suppressed or promoted PI3P production, respectively, as defined by GFP-FYVE, a PI3P-binding reporter (Figures 2A and S2A–S2C). Specifically, overexpression of p300, but not the other acetyltransferases, dramatically decreased PI3P production, while deletion of p300 increased it (Figures 2B, 2C, and S2D), suggesting a negative effect of p300 on VPS34 activity. In vitro lipid kinase assays then confirmed this effect. Purified bovine PI was incubated with VPS34 immunoprecipitated from CTB- or C646-treated cells in the presence of γ-^{32}P-ATP, and the extracted phospholipid products were separated by thin-layer chromatography. Production of ^{32}P-PI3P was inversely related to p300 activity (Figure 2D). In vitro PI3P ELISA assay using PI and VPS34 immunoprecipitated from DCA- or UK5099-treated cells acquired consistent results (Figure S2E). Furthermore, VPS34 from cells with a deletion of p300 demonstrated much stronger PI3P-producing activity, which was neutralized by expression of WT p300, but not inactive p300 (Figure 2E). These data demonstrate that VPS34 is inhibited by p300 in vitro and in cells. We then created acetylation-disabled lysine-to-arginine (VPS34-KR) and acetylation-mimetic lysine-to-glutamine

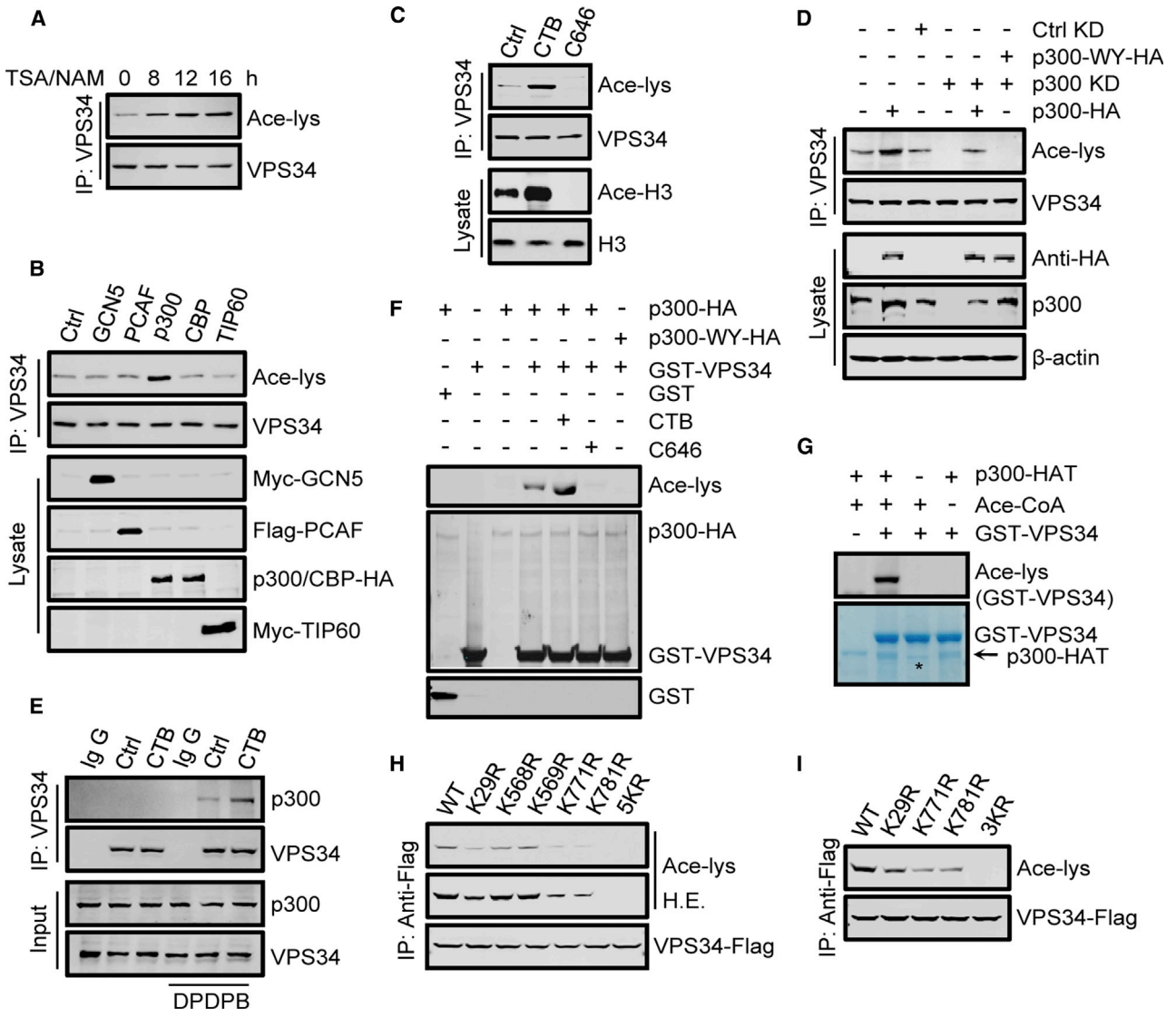

Figure 1. VPS34 Is Acetylated by p300 at K29, K771, and K781

(A) Acetylation of VPS34 in HEK293 cells treated with the deacetylase inhibitors TSA and NAM. VPS34 was immunoprecipitated from cell lysates with an anti-VPS34 antibody, then analyzed by immunoblot using an anti-acetyl-lysine antibody (Ace-lys).

(B and C) VPS34 acetylation in HEK293 cells overexpressing the indicated individual histone acetyltransferases (B) or treated with the p300 activator CTB or the p300 inhibitor C646 (C). H3, Histone3; Ace-H3, acetyl-histone3 (Lys56).

(D) VPS34 acetylation in HEK293 cells transfected with p300-HA or the acetyltransferase-dead p300-WY-HA after 48 hr incubation with p300 siRNA.

(E) Association of p300 with VPS34. VPS34 was immunoprecipitated from HEK293 cells treated with or without the cross-linker DPDPB, and the precipitates were analyzed using anti-p300.

(F) In vitro acetylation assays using purified GST-VPS34 and HA-tagged p300 or p300-WY immunoprecipitated from treated HEK293T cells.

(G) In vitro acetylation assays using purified GST-VPS34 and p300 HAT domain. The arrow indicates the band of p300-HAT domain. Asterisk indicates non-specific band.

(H and I) Acetylation of Flag-tagged VPS34 or VPS34 mutants expressed in cells. 5KR, all five Lys residues were replaced by Arg; 3KR, Lys 29, Lys 771, and Lys 781 were replaced by Arg. H.E., high exposure.

(VPS34-KQ) mutants at K29, K771, and K781, either individually or together. When expressed in cells, all the VPS34-KQ mutants reduced the numbers of GFP-FYVE puncta (Figure 2F), while K771R enhanced, and the triple replacement (3KR) maximized, the formation of GFP-FYVE puncta (Figure 2F). In support of these findings, in vitro lipid kinase assays showed that the VPS34 mutants consistently converted PI into PI3P (Figures 2G and 2H). Together, these results suggest that deacetylation of VPS34 is required for its activation. The effects of deacetylation at K29, K771, and K781 are synergistic, and deacetylation at K771, which is located in the catalytic domain, may play a dominant role.

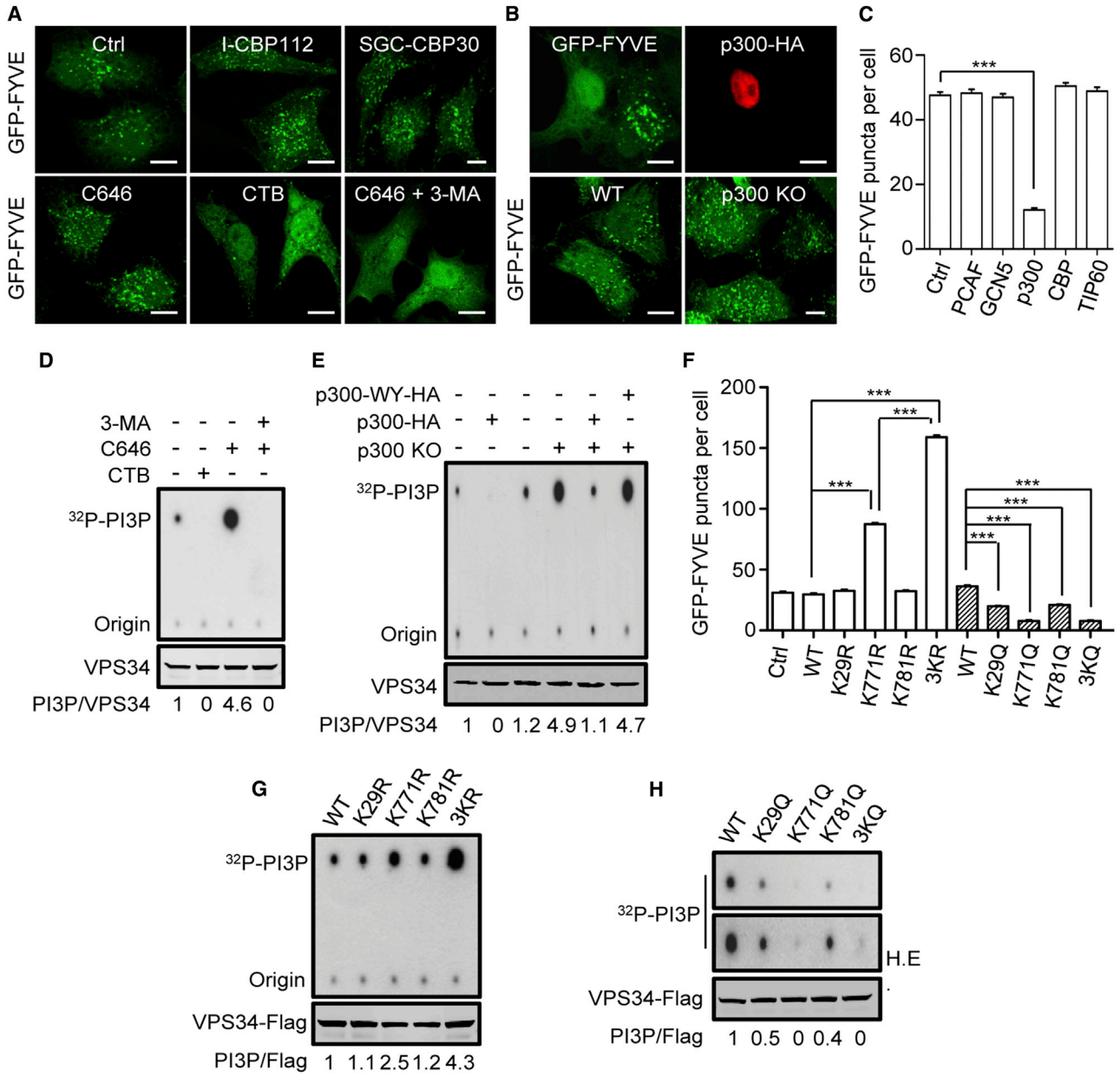

Figure 2. Acetylation by p300 Inactivates VPS34

(A) Distribution of GFP-FYVE in HEK293 cells treated with the p300 activator CTB or the p300 inhibitor I-CBP112, SGC-CBP30, or C646, with or without the VPS34 inhibitor 3-MA.

(B) GFP-FYVE distribution in p300-HA-overexpressing or p300-KO HEK293 cells.

(C) Quantification of GFP-FYVE puncta in HEK293 cells overexpressing different acetyltransferases.

(D and E) In vitro lipid kinase assays of VPS34 immunoprecipitated from C646- and CTB-treated HEK293 cells (D), and from p300-KO HEK293 cells with or without p300-HA or p300-WY-HA transfection (E).

(F) Quantification of GFP-FYVE puncta in HEK293 cells co-transfected with plasmids expressing WT VPS34 and different KR and KQ mutants.

(G and H) In vitro lipid kinase assays of the Flag-tagged VPS34 mutants immunopurified from transfected HEK293T cells. H.E., high exposure. Relative ratios of the ^{32}P-PI3P signal divided by the VPS34 protein signal are shown in (D), (E), (G), and (H). Scale bar, 10 μm. The statistical results are shown as mean ± SEM, n = 30. ***p < 0.001. 3KR, Lys 29, Lys 771, and Lys 781 were replaced by Arg; 3KQ, Lys 29, Lys 771, and Lys 781 were replaced by Gln.

Acetylation at K29 Inhibits VPS34-Beclin 1 Association

Mounting evidence suggests that the activity of VPS34 is controlled by interaction with its regulatory protein Beclin 1. To investigate the mechanism by which acetylation inhibits VPS34, we first investigated the VPS34-Beclin 1 interaction. CTB treatment or p300 overexpression attenuated, whereas C646 treatment or p300-KO enhanced, the co-immunoprecipitation of Beclin 1 rather than p150 with VPS34 (Figures 3A and 3B).

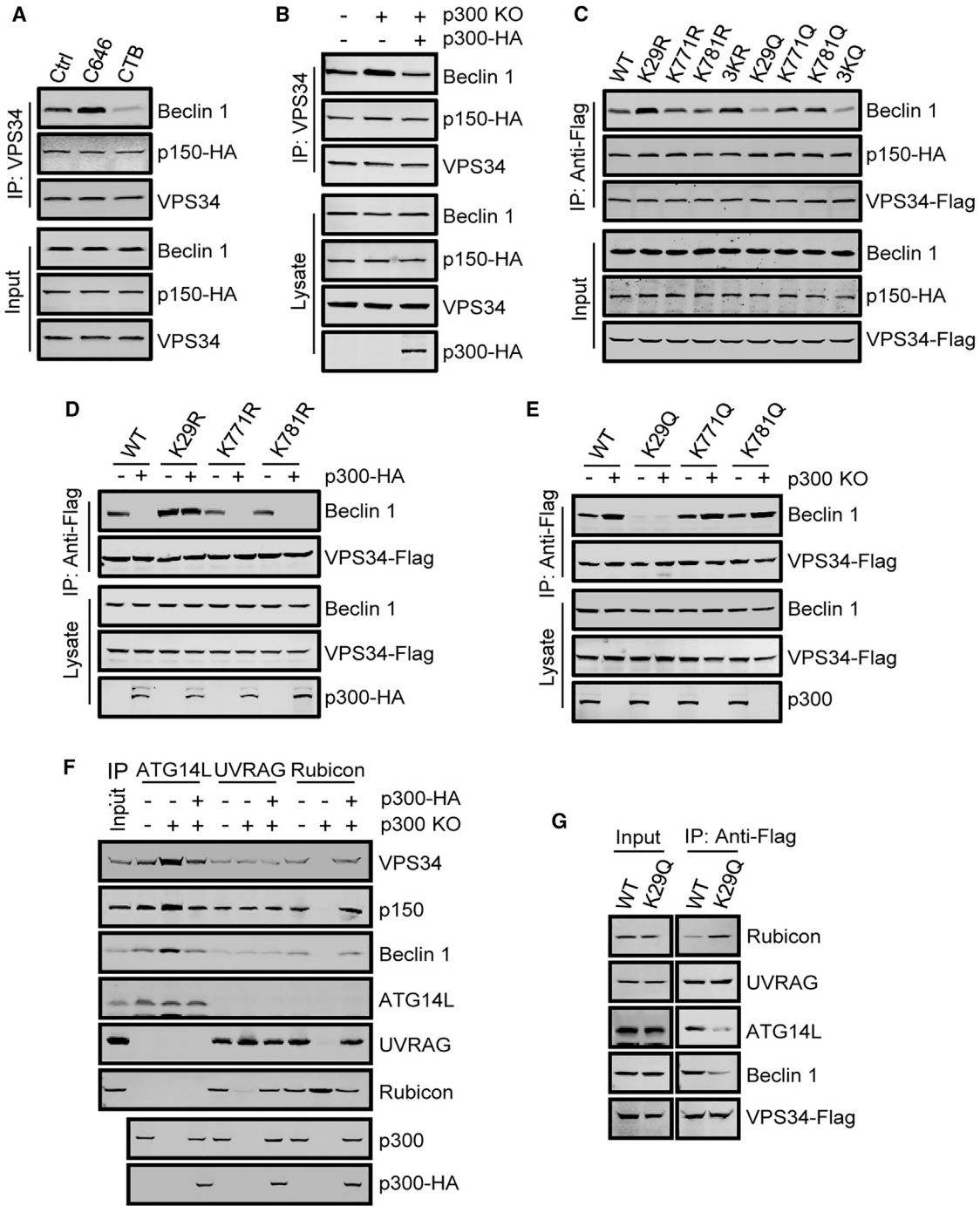

Figure 3. Acetylation at K29 Inhibits VPS34-Beclin 1 Association

(A) Co-immunoprecipitation of Beclin 1 and p150-HA with VPS34. VPS34 was immunoprecipitated from HEK293 cells expressing p150-HA, and the precipitates were analyzed using anti-Beclin 1 or anti-HA.

(B) Co-immunoprecipitation of Beclin 1 and p150-HA with VPS34 in p300-KO HEK293 cells with or without p300-HA expression.

(C) Co-immunoprecipitation of Beclin 1 and p150-HA with Flag-tagged VPS34 mutants in co-transfected HEK293 cells. Immunoprecipitation was carried out with anti-Flag, and the precipitates were immunoblotted with anti-Beclin 1 or anti-HA.

(D and E) Co-immunoprecipitation of Beclin 1 with VPS34-Flag mutants in HEK293 cells with or without p300-HA expression (D) or p300 deletion (E).

(F) p300-KO HEK293 cells were transfected with or without p300-HA, and the cell lysates were subjected to immunoprecipitation using antibody against ATG14L, UVRAG, or Rubicon. Then the precipitates were examined by immunoblotting with the indicated antibodies.

(G) Co-immunoprecipitation of Rubicon, UVRAG, ATG14L, and Beclin 1 with Flag-tagged WT VPS34 or K29Q in HEK293 cells. 3KR, Lys 29, Lys 771, and Lys 781 were replaced by Arg; 3KQ, Lys 29, Lys 771, and Lys 781 were replaced by Gln.

This suggests that VPS34 deacetylation, mediated by p300 inhibition, increases the VPS34-Beclin 1 association. Intriguingly, expression of each of the acetylated K-to-Q or deacetylated K-to-R mutants in cells revealed that the K29R mutation increased and the K29Q mutation decreased VPS34-Beclin 1 co-immunoprecipitation (Figure 3C). Mutation at K771 or K781 barely affected the VPS34-Beclin 1 association, and none of the mutations changed the VPS34-p150 co-immunoprecipitation (Figure 3C). These results imply that only acetylation at K29 is relevant to the VPS34-Beclin 1 interaction. To test this, we checked the mutants for Beclin 1 binding in p300-transfected and p300-KO cells. It was evident that p300 overexpression abolished the association of WT VPS34 or the K771R or K781R mutant with Beclin 1, while the association between the K29R mutant and Beclin 1 was not affected (Figure 3D). In line with this, p300 deletion augmented the binding of WT or the K771Q or K781Q mutant to Beclin 1 but failed to rescue the suppressed association of the K29Q mutant with Beclin 1 (Figure 3E). Together, these results suggest that deacetylation at K29, but not at K771 and K781, is crucial for the VPS34-Beclin 1 association. K29 is located in the N-terminal C2 domain, which interacts with Beclin 1 (Liang et al., 2006), while K771 and K781 are in the catalytic domain.

In mammalian cells, there are at least three complexes that contain VPS34-p150-Beclin 1 core and are involved in different cellular processes. VPS34-p150-Beclin 1-ATG14L complex is required for the formation of autophagosomal precursor by producing PI3P in the endoplasmic reticulum (Itakura et al., 2008; Matsunaga et al., 2010); VPS34-p150-Beclin 1-UVRAG complex regulates endocytic trafficking by driving endosomal tethering and fusion (Itakura et al., 2008; McKnight et al., 2014), and it also plays a role in autophagosome-lysosome fusion (Cheng et al., 2017; Matsunaga et al., 2009); VPS34-p150-Beclin 1-UVRAG-Rubicon complex is related to both the endolysosomal and autophagic functions through the inhibitory effect of Rubicon on VPS34 (Matsunaga et al., 2009; Zhong et al., 2009). To determine the effect of p300-mediated VPS34 acetylation on the formation of these complexes in cells, we carried out immunoprecipitation using anti-ATG14L, anti-UVRAG, and anti-Rubicon separately. Deletion of p300 enhanced the interaction of ATG14L with the VPS34-p150-Beclin 1 core and abolished the binding of Rubicon and the core, both of which could be reversed by p300 re-expression (Figure 3F). The association of UVRAG with VPS34-p150-Beclin 1 core complex was not affected by the expression level of p300 (Figure 3F). Consistently, immunoprecipitation of the K29Q mutant co-precipitated less ATG14L, more Rubicon, and equal amounts of UVRAG, compared to that of WT VPS34 (Figure 3G). These results suggest that VPS34 acetylation-regulated VPS34-Beclin 1 interaction can differentially affect the formation of distinct VPS34-p150-Beclin 1 core-based complexes. While the enhanced VPS34-Beclin 1 interaction by K29 deacetylation increases the recruitment of ATG14L through Beclin 1-ATG14L binding (Sun et al., 2011), K29 acetylation may promote the interaction between Rubicon and VPS34 (Sun et al., 2011).

Acetylation at K771 Disrupts VPS34-PI Interaction

We next determined how acetylation at K771 and K781 reduces VPS34 activity. Structurally, the activation loop of VPS34 is fully ordered and is made up of three residues from the catalytic domain, Y764, P770, and K771, which together are responsible for binding the substrate PI (Miller et al., 2010). The K-to-Q, but not K-to-R, replacement at K771 is predicted to shorten the activation loop (Figure 4A). This suggests that acetylation at K771, and not just the amino acid substitution, may influence the integrity of the loop. To test a potential effect of acetylation at K771 and the structurally adjacent residue K781 on VPS34-PI binding, liposomes containing PI (Burke et al., 2012) were constructed and incubated with purified recombinant GST-tagged WT VPS34 or the K-to-Q protein mutants. We found that the K29Q mutant associated with the liposomes, as did the WT, whereas the K781Q mutant bound less effectively and the K771Q mutant barely bound at all (Figures 4B and 4C). To confirm specific VPS34-PI binding to the liposomes and further analyze the affinity of VPS34 for PI, we performed protein-lipid overlay assays. As expected, the K29Q mutation hardly influenced the VPS34-PI association, while the K781Q mutation attenuated it and K771Q abolished it (Figure 4D). The fact that the K771R mutant and WT VPS34 bound to PI to a similar degree validated the specific effect of acetylation, but not amino-acid substitution (Figure 4D). These results support previous data showing that the C2 domain has no influence on VPS34 catalytic activity in vitro (Miller et al., 2010). More importantly, they suggest that K771 within the catalytic domain is pivotal for the VPS34-PI interaction.

Deacetylation of VPS34 Is Required for Nutrient-regulated Autophagy

To evaluate the physiological significance of p300-dependent VPS34 acetylation, we tested its function in autophagy, since autophagosome formation requires production of PI3P by VPS34. The autoacetylation of p300 protein reflects its acetyltransferase activity (Thompson et al., 2004). Inactivation of p300 (indicated by p300 deacetylation) and deacetylation of VPS34 were found in cells starved of amino acids or glucose, or after treatment with the mTORC1 inhibitor Torin1 (Figure 5A). CTB pretreatment prevented VPS34 deacetylation and reduced the specific autophagic pool of PI3P stimulated by cell starvation, as indicated by GFP-DFCP1 puncta that localized to omegasomes (Axe et al., 2008) (Figures 5A, 5B, and S3A). We then expressed the VPS34 mutants in cells and measured their activity by in vitro kinase assays. Amino acid starvation significantly activated WT VPS34 but failed to further increase the activity of the fully deacetylated mutant, suggesting that VPS34 is sufficiently activated by the deacetylation (Figure 5C). Notably, the K29Q mutant was partially activated, while the K771Q mutant and the fully acetylated mutant (3KQ) remained completely inactive (Figures 5C and 2H). The activity of the mutants on the production of autophagic PI3P was verified by expressing each of them in the VPS34 knockdown cell and counting the formation of GFP-DFCP1 puncta (Figures S3B and S3C). Amino acid starvation did not promote the interaction of the K29Q mutant with Beclin 1 or ATG14L (Figure S3D), suggesting that the increased activity of the K29Q mutant in PI3P production under amino acid deprivation comes from the deacetylation at K771 and K781. Together, these results confirmed that VPS34 activation requires VPS34 deacetylation during nutrient-regulated autophagy.

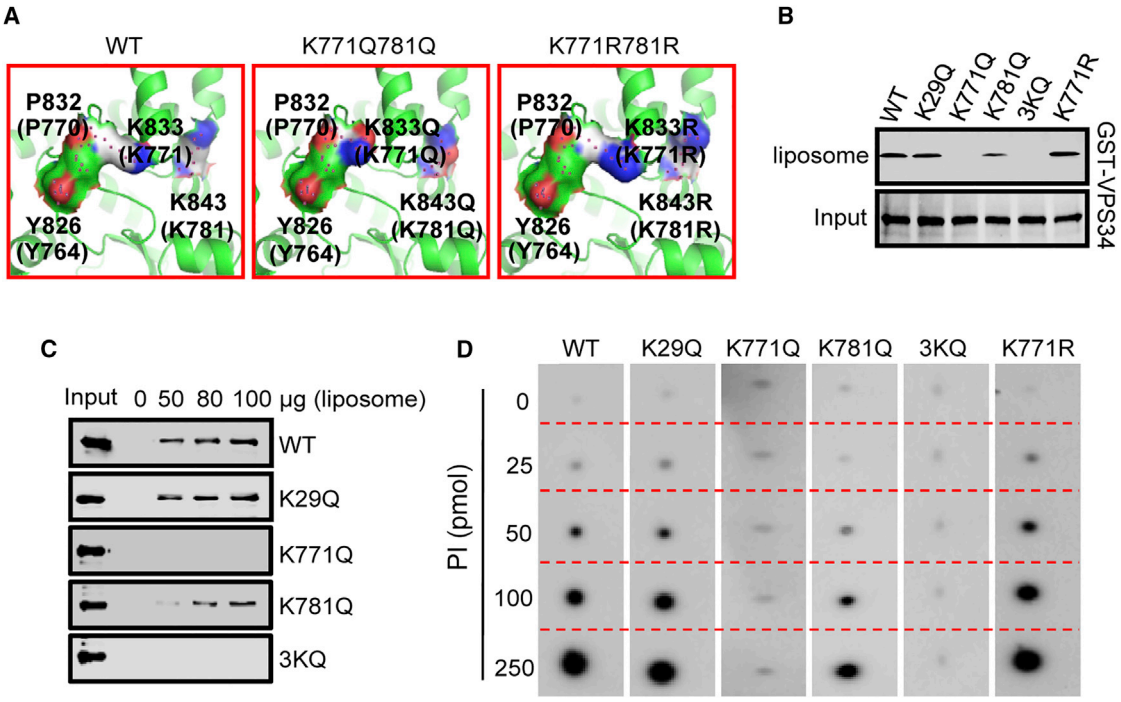

Figure 4. Acetylation at K771 Disrupts VPS34-PI Interaction

(A) The hook-shaped activation loop of *Drosophila* VPS34 comprising Y826, P832, and K833, which correspond to Y764, P770, and K771, respectively, in human VPS34. Images were created using Pymol (http://www.pymol.org) and Protein Data Bank (PDB) accession 2X6H.

(B and C) Liposome-binding assays of VPS34 proteins. Liposomes containing PI were cultured with purified GST-VPS34 or GST-VPS34 mutants, then ultracentrifuged and analyzed by immunoblot with anti-GST.

(D) Analysis of the binding of purified VPS34 mutant proteins with PI by protein-lipid overlay assays. Note that there is no detectable association between K771Q and PI. 3KQ, Lys 29, Lys 771, and Lys 781 were replaced by Gln.

To determine whether autophagy was regulated accordingly in cells, we constructed a K29Q/K771R/K781R mutant that bound PI and had a reduced affinity for Beclin 1, and a K29R/K771Q/K781Q mutant that interacted with Beclin 1 but not PI (Figures 3D and 4D). We checked the capacity of these mutants to rescue VPS34 RNAi-induced inhibition of autophagosome formation, GFP-LC3 processing, p62 degradation, and lactate dehydrogenase (LDH) sequestration (Luhr et al., 2017) in cells. VPS34 RNAi blocked the autophagosome formation (Figures 5D–5F), GFP-LC3 cleavage (Figure 5G), p62 degradation (Figure 5H), and LDH sequestration (Figure 5I) triggered by amino acid depletion. Transfection of WT VPS34 completely reversed the effects of VPS34 RNAi, and K29QK771RK781R partially but significantly rescued these effects, while K29RK771QK781Q completely failed to do so (Figures 5E–5I). Similar results were obtained in glucose-starved cells (Figures S3E–S3I). The triggered p62 reduction by overexpression of WT VPS34 or the K29QK771RK781R mutant was fully blocked by a lysosome inhibitor chloroquine (CQ) and confirmed an autophagic degradation of p62 (Figures 5H and S3I).

Acetylation of VPS34 at K29 increased the interaction of Rubicon with VPS34-p150-Beclin 1 core (Figures 3F and 3G), suggesting a potential effect of VPS34 acetylation on the late stage of autophagy and endocytic trafficking. We then observed the sites of PI3P accumulation by assessing the co-localization of GFP-FYVE puncta with Rab5 (early endososme marker) and Rab7 (late endososme/lysosome marker). Under normal conditions, GFP-FYVE co-localized with Rab5 but rarely with Rab7 or LC3 (Figure S4A). Upon C646 treatment, the increase in GFP-FYVE numbers was accompanied by enhanced co-localization of GFP-FYVE with all the markers (Figures S4A and S4B). We also checked the impact of VPS34 acetylation on LC3-Lamp1 co-localization by expressing the acetylation-mimicking VPS34 mutants in VPS34-knockdown cells. Consistent with the results showing in Figure 5E, amino acid starvation stimulated the formation of GFP-LC3 puncta in cells expressing WT VPS34 or the K29Q mutant (Figure S4C). However, LC3-Lamp1 co-localization was dramatically inhibited in K29Q-expressing cells when compared with cells expressing WT VPS34 (Figures S4C and S4D). Finally, the acetylation-mimicking VPS34 mutants were transfected to cells, and the degradation of cellular EGFR was analyzed. Apparently, EGFR degradation was impaired by K29Q overexpression and was blocked by K771Q overexpression (Figure S4E). Taken together, these results suggest that deacetylation of VPS34 is essential for nutrient-regulated autophagy as well as endocytic transport.

Inhibition of p300 Activates VPS34 and Autophagy in *AMPK*$^{-/-}$, *TSC2*$^{-/-}$, and *ULK1*$^{-/-}$ Cells

Recently, non-canonical forms of autophagy have been discovered in which the signal from AMPK (Grotemeier et al., 2010), mTORC1 (Lipinski et al., 2010; Yamamoto et al., 2006), ULK1 (Cheong et al., 2011), or even Beclin 1 (Smith et al., 2010) is

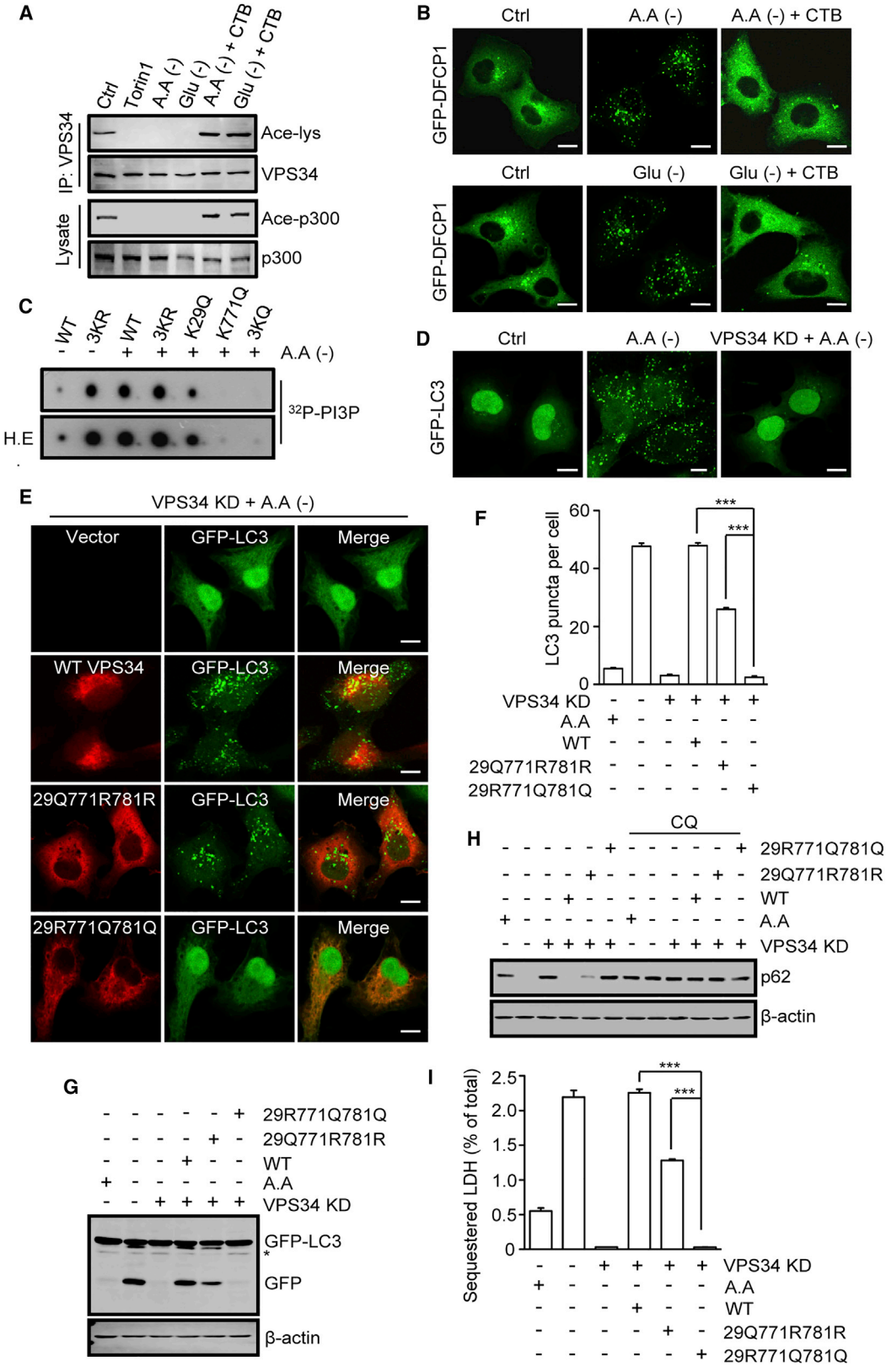

(legend on next page)

dispensable for autophagosome formation. We therefore investigated the possible involvement of the p300-VPS34 pathway in these processes. VPS34 activation and autophagosome formation and autophagic flux were examined in cells in which the individual proteins upstream of VPS34 were genetically deleted and p300 was also inactivated by its inhibitors or RNAi. Strikingly, inactivation of p300 stimulated autophagic PI3P in *AMPK*$^{-/-}$, *TSC2*$^{-/-}$ (with high constitutive mTORC1 activity), *ULK1*$^{-/-}$, and *FIP200*$^{-/-}$ (lacking ULK1 activity) cells, but not in *Beclin 1*$^{-/-}$ cells (Figures 6A and S5A–S5F). Meanwhile, the formation of LC3 puncta (Figures 6B and S5G–S5I), degradation of p62 (Figure 6C), the generation of lipidated LC3-II from LC3-I (Figure 6C), and sequestration of LDH (Figure S6A) were clearly elevated, although less than in WT cells. Further, we analyzed VPS34 activity and autophagy in cells treated with ammonia, which is generated by normal catabolism of proteins and nucleic acids and induces autophagy independent of ULK1/2 (Cheong et al., 2011). In the gene-deleted cells, addition of NH_4Cl at a low concentration which does not inhibit lysosomes (Cheong et al., 2011; Eng et al., 2010) led to marked p300 inactivation and VPS34 deacetylation (Figure 6D). Meanwhile, autophagic PI3P production was activated (Figure 6E) and was accompanied by an increase in autophagosome formation (Figure 6F), p62 degradation, and LC3-II production (Figure S6B); all of these were abolished by CTB pretreatment. Finally, we overexpressed WT VPS34 or the acetylation-mimicking 3KQ mutant in the gene-deleted cells and observed the role of VPS34 acetylation on autophagosome formation. Significantly, 3KQ, but not WT VPS34, inhibited the production of LC3 puncta in cells stimulated by C646 treatment or p300 RNAi (Figures 6G, S6C, and S6D). Together, these data suggest that p300 inhibition mediates VPS34 deacetylation and activation in non-canonical autophagy. With regard to the exceptional requirement for Beclin 1, ATG14L protein was lacking in *Beclin 1*$^{-/-}$ cells, but not in the other KO cells (Figure 6H), supporting a role of Beclin 1 in stabilizing ATG14L (Kihara et al., 2001; Itakura et al., 2008). The loss of ATG14L in *Beclin 1*$^{-/-}$ cells might explain why they failed to produce autophagic PI3P and form autophagosomes in response to p300 inactivation (Matsunaga et al., 2010).

p300 Inactivation and VPS34 Deacetylation in Liver Autophagy and in Hepatocyte Lipid Droplet Clearance

We then assessed the role of this p300-VPS34 pathway in autophagy in fasting mice. p300 activity, VPS34 acetylation, and autophagy were analyzed in liver tissue of mice starved of nutrients for 24 hr (Mizushima et al., 2004). Liver autophagy was stimulated by starvation, as shown by the formation of LC3 puncta and reduction of p62 protein levels (Figures 7A and 7B). Meanwhile, the acetylation of liver p300 and VPS34 decreased, indicating that p300 was inactivated and VPS34 was activated (Figure 7C). Strikingly, CTB treatment prevented starvation-induced VPS34 deacetylation and autophagy, while C646 treatment alone effectively triggered VPS34 deacetylation and autophagy in the liver of fed mice (Figures 7A–7C). The C646-stimulated degradation of liver p62 was blocked by CQ, indicating a dependence on autophagy (Figure S7A). To gain direct evidence that VPS34 acetylation regulates autophagy in liver, mice were intraperitoneally injected with recombinant adeno-associated virus (rAAV) expressing wild-type VPS34 (rAAV-WT), 3KR (rAAV-3KR), or 3KQ (rAAV-3KQ), and the mice were starved for 24 hr. Administration of rAAV-3KQ significantly inhibited starvation-induced autophagosome formation and p62 degradation, accompanied by dramatic accumulation of lipids in the liver tissues, while rAAV-WT or rAAV-3KR injection did not show marked effect (Figures 7D–7F and S7B). We also evaluated the function of p300-VPS34 pathway in breakdown of intracellular lipid droplets (LDs) in hepatocytes. In L02 cells, serum starvation and different p300 inhibitors significantly reduced cellular LDs (Figures 7G and S7C–S7E). When the serum starvation-induced LD reduction was blocked by CTB, the LD reductions by p300 inhibitors were prevented by ATG5 or ATG7 RNAi (Figures 7G and S7C–S7E). In addition, the serum starvation-induced LD breakdown was promoted by VPS34-3KR expression and was prevented by VPS34-3KQ expression, also by CQ treatment or ATG7 RNAi (Figures 7H and S7F–S7H). These results therefore support a physiological role of p300 inactivation and consequent VPS34 deacetylation in autophagy in vivo and autophagy-related clearance of lipid droplets in hepatocytes.

DISCUSSION

Here we have found a previously unknown pathway for regulating the activation of the lipid kinase VPS34. Our results indicate that acetylation directly controls the kinase activity of VPS34 and the formation of complexes with its regulatory proteins. We propose that this acetylation/deacetylation-based mechanism is involved in other VPS34-dependent membrane processes as well as the initiation of autophagy.

Figure 5. VPS34 Deacetylation Is Required for Nutrient Starvation-Induced Autophagy

(A) Acetylation of VPS34 and p300 in HEK293 cells treated with Torin 1 or amino acid- or glucose-free medium for 4 hr in the presence or absence of the p300 activator CTB.

(B) Distribution of GFP-DFCP1 in HEK293 cells with amino acid or glucose starvation for 4 hr in the presence or absence of CTB.

(C) In vitro lipid kinase assays of VPS34 and VPS34 mutant proteins immunopurified from transfected HEK293 cells undergoing amino acid starvation. H.E., high exposure.

(D) Images of amino acid-starved GFP-LC3-stable HEK293 cells with or without VPS34 RNAi.

(E) GFP-LC3 puncta in amino acid-starved VPS34 siRNA-cultured GFP-LC3-stable HEK293 cells, with or without transfection of Flag-tagged VPS34 or VPS34 mutants 48 hr after VPS34 RNAi.

(F) Quantification of GFP-LC3 puncta in GFP-LC3-stable HEK293 cells treated as in (D) and (E). Data are presented as mean ± SEM, n = 30. ***$p < 0.001$.

(G) Immunoblot for detection of the free GFP fragment using anti-GFP antibody in GFP-LC3-stable HEK293 cells treated as in (D) and (E). Asterisk indicates non-specific band.

(H) Immunoblot showing intracellular p62 levels in HEK293 cells treated as in (G) with or without addition of chloroquine (CQ).

(I) LDH sequestration assay in HEK293 cells treated as in (G) with addition of CQ. Data are presented as mean ± SEM of triplicates. Scale bar, 10 μm.

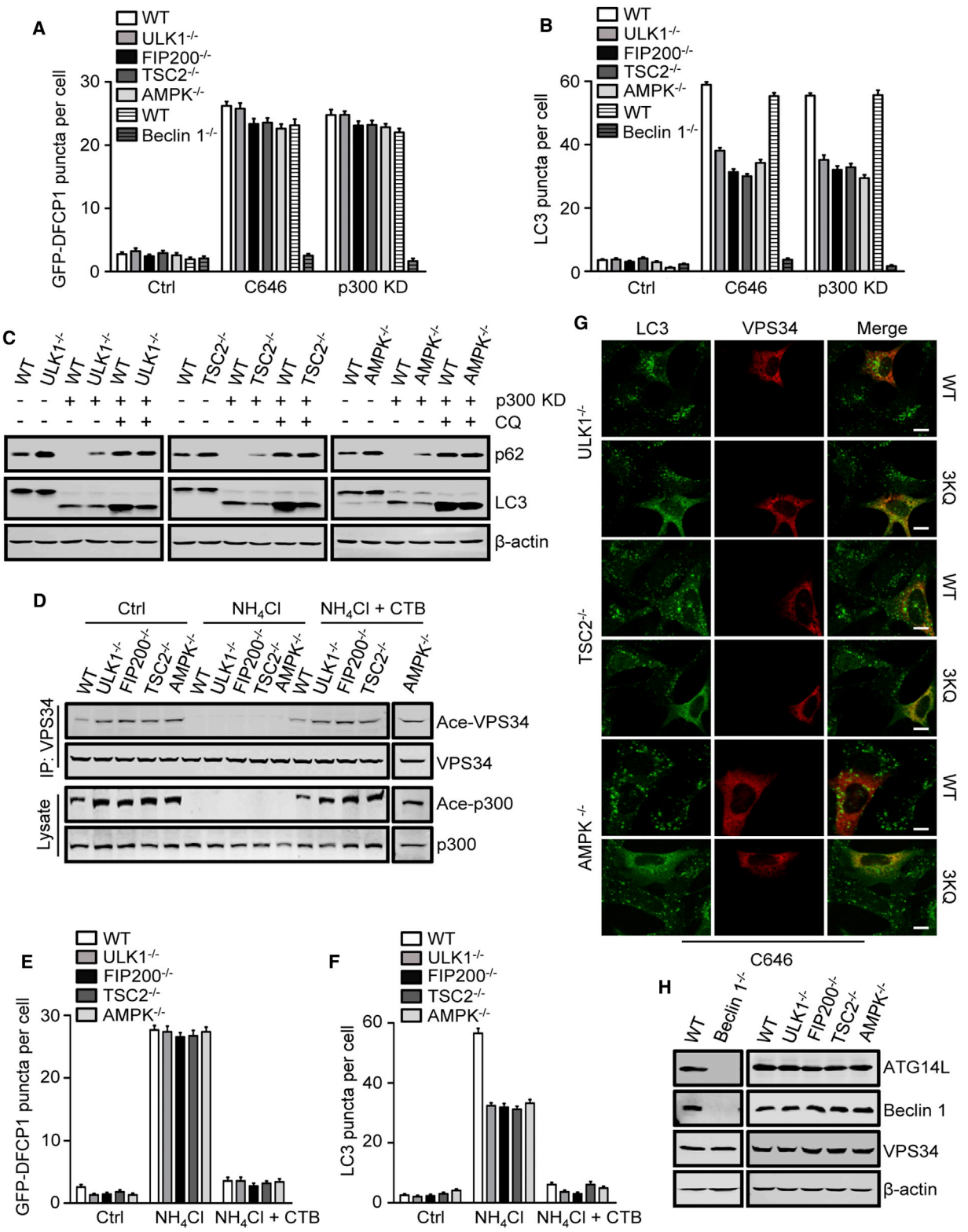

Figure 6. p300-mediated VPS34 Acetylation in Non-canonical Autophagy

(A and B) Quantification of GFP-DFCP1 puncta (A) and LC3 puncta (B) in gene-deleted MEFs and Beclin 1-deleted HEK293 cells with or without C646 treatment or p300 RNAi. Data are presented as mean ± SEM, n = 30.

(C) Immunoblot assay of intracellular p62 and LC3 in the gene-deleted MEFs. The cells were treated with p300 siRNA with or without CQ (10 μM).

(legend continued on next page)

Combined with previous findings showing the effect of AMPK on Sirt1 (Cantó et al., 2009; Chang et al., 2015) and p300 on mTOR (Pietrocola et al., 2015a), our data verify a cross-talk between protein phosphorylation-controlled PI3P production and the protein acetylation-regulated LC3-PE conjugation. In fact, in *TSC2*$^{-/-}$, *ULK1*$^{-/-}$, and *FIP200*$^{-/-}$ cells, acetylation of p300 is clearly elevated (as shown in Figure 6D), suggesting that p300 may be positively regulated by mTOR and negatively regulated by ULK1, as it is by AMPK (Zhang et al., 2011; Yang et al., 2001). While the possibility that p300 may act on the kinases upstream of VPS34 cannot be ruled out at this time, our results indicate that VPS34 is a direct target of p300 (Figure 7I). This mechanism ensures that VPS34 is activated for autophagy initiation not only under conditions like nutrient deficiency, which can use the canonical AMPK-mTORC1-ULK1 route, but also in situations where the upstream regulatory kinases are not affected or missing. It is noteworthy that this p300-VPS34 pathway is also required for nutrient deficiency-induced VPS34 activation and autophagy in which the AMPK-mTORC1-ULK1 route is available. This rules out the possibility that failure of autophagy induction by increased p300 activity is caused merely by inadequate levels of LC3 lipidation, and more importantly it suggests that VPS34 deacetylation has a pivotal role in both canonical and non-canonical autophagy. The data also provide additional evidence that downregulation of p300 is necessary and sufficient for autophagy induction (Lee and Finkel, 2009; Pietrocola et al., 2015a). Considering that intracellular acetyl-CoA is a major and direct regulator of p300, and acetyl-CoA has been proposed as a central metabolite messenger (Pietrocola et al., 2015b), our study suggests that p300 may serve as a protein responder to the change in intracellular energy status by modulating cell metabolism, including the initiation of autophagy.

Identification of K29 and K771 as the acetylation and deacetylation sites leads to the discovery of a novel molecular mechanism for the regulation of VPS34 activation. VPS34 can undergo sumoylation and phosphorylation (Kim et al., 2013; Yang et al., 2013). So far, these modifications all alter VPS34 activity by affecting the formation of VPS34 complexes, which resembles the effect of upstream regulatory kinases on VPS34. Our results show that acetylation at K771 directly affects the affinity between VPS34 and its substrate PI, thus uncovering a previously unknown avenue for VPS34 activation. Compared with K29 deacetylation, which affects the VPS34-Beclin 1 interaction, the dominant role of K771 deacetylation suggests that it is a critical step for VPS34 activation after the VPS34 complex is assembled at or recruited to membranes. Acetylation at K771 probably disrupts the contact between K771 and the 1-phosphate in the inositol ring of PI by neutralizing the positive charge of the lysine side chain, as it has been speculated that the 1-phosphate is structurally adjacent to the ε-amino group of K771 (Miller et al., 2010). K29 and K771 are far apart from each other on VPS34, and it is unknown currently whether p300 acetylates the sites contemporarily or sequentially. Nevertheless, our results demonstrating that mutation at each of the sites only partially decreased VPS34 acetylation level suggests that the acetylations may not be sequential. It is known that activation of p300 depends on its autoacetylation, which suggests a dimerization of p300 in the process (Thompson et al., 2004; Karanam et al., 2006). A possible explanation for the acetylation at the far-apart sites may be that one of the dimerized p300 acetylates K29 when the other acetylates K771.

Although the canonical upstream kinases of VPS34 can be bypassed, our results demonstrate that Beclin 1 is indispensable for VPS34 activation in cells. We show that this is due to the function of Beclin 1 in stabilization of ATG14L, possibly by covering the ubiquitination sites on ATG14L (Kihara et al., 2001; Zhang et al., 2015). Interestingly, induction of Beclin 1-independent autophagy has been reported in different cell types, especially by apoptosis-stimulating chemicals (Zhu et al., 2007; Tian et al., 2010; Scarlatti et al., 2008). Presumably, for autophagy triggered by these chemicals, PI3P is produced either by inhibition of its phosphatase (Taguchi-Atarashi et al., 2010) or by dephosphorylation of PI(3,5)P_2 (Rudge et al., 2004). Alternatively, instead of PI3P, synthesis of PI5P can serve as the nucleator for the generation of isolation membranes (Vicinanza et al., 2015). Our results demonstrate that in cells with deletion of the upstream kinases of VPS34, p300 inactivation leads to full VPS34 activation and partial autophagosome formation compared to wild-type cells. The reduced autophagosome formation may be attributed to the lack of ULK1 activity, because in addition to VPS34 activation the ULK1 complex is also responsible for the recruitment of ATG16, which contributes to LC3-PE conjugation (Fujita et al., 2008; Nishimura et al., 2013).

STAR★METHODS

Detailed methods are provided in the online version of this paper and include the following:

- KEY RESOURCES TABLE
- CONTACT FOR REAGENT AND RESOURCE SHARING
- EXPERIMENTAL MODEL AND SUBJECT DETAILS
  - Cell culture
  - Stable cell lines construction
  - Mice feeding
- METHOD DETAILS
  - Reagents
  - Transfection
  - Cell imaging
  - Immunoblot and immunoprecipitation
  - Recombinant protein purification and in vitro acetylation assay
  - Subcellular fractionation
  - Fluorometric acetyl-CoA quantitation assay
  - HPLC-MS/MS
  - Analysis of tandem mass spectra

(D) Acetylation of VPS34 and p300 in gene-deleted MEFs treated with NH_4Cl with or without CTB pretreatment.
(E and F) Quantification of GFP-DFCP1 puncta (E) and LC3 puncta (F) in gene-deleted MEFs treated as in (D). Data are presented as mean ± SEM, n = 30.
(G) Formation of LC3 puncta in C646-treated gene-deleted MEFs overexpressing Flag-tagged WT VPS34 or 3KQ. Scale bar, 10 μm.
(H) Expression of the indicated proteins in gene-deleted MEFs and Beclin 1-deleted HEK293 cells. Note the loss of ATG14L in Beclin 1-deleted cells.

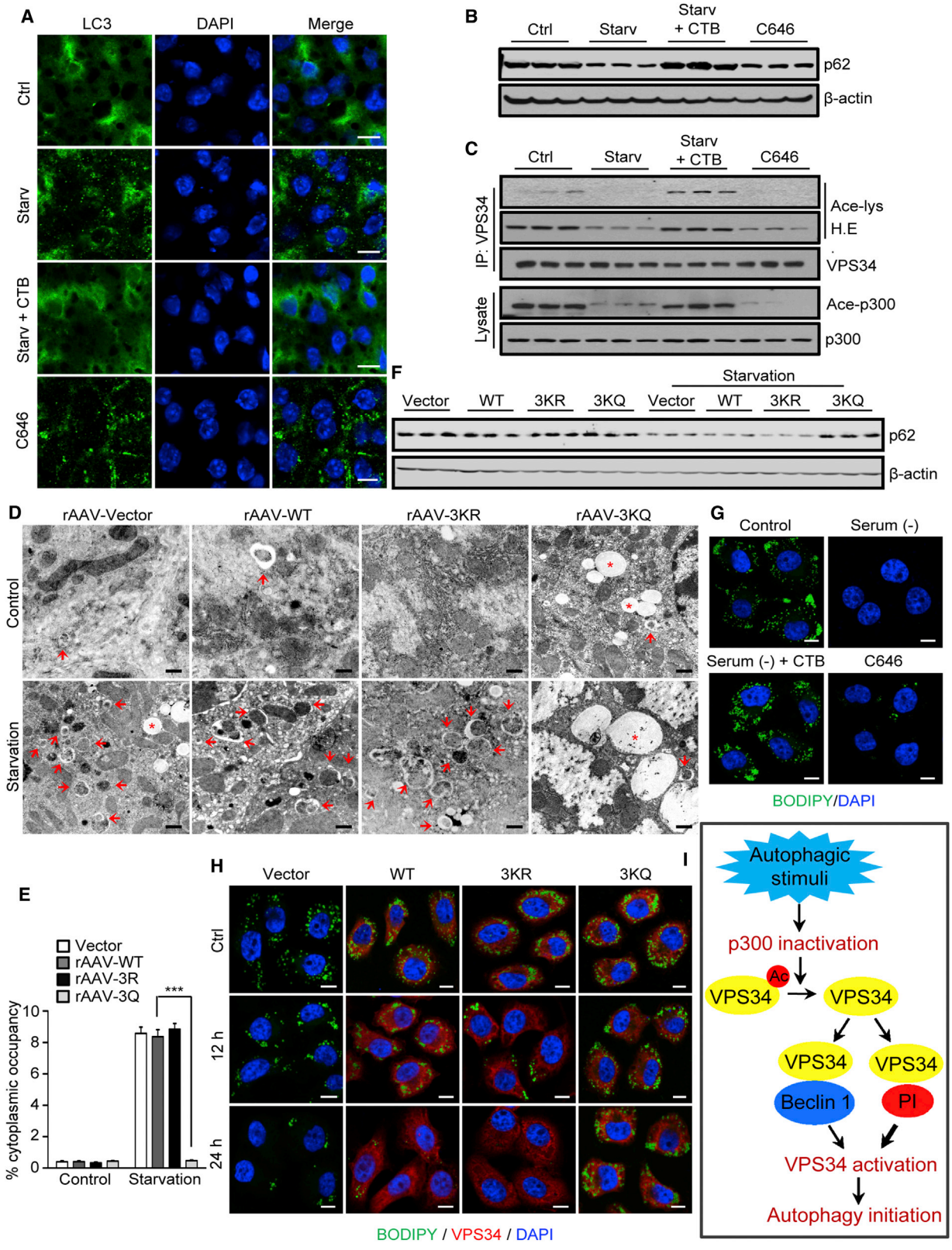

(legend on next page)

- In vitro VPS34 lipid kinase assay
- In vitro PI3P ELISA assay
- Liposome preparation and liposome sedimentation assay
- Protein-lipid overlay assay
- LDH sequestration assay
- EGFR degradation assay
- Mouse experiments and tissue processing
- Transmission electron microscopy

● QUANTIFICATION AND STATISTICAL ANALYSIS

SUPPLEMENTAL INFORMATION

Supplemental Information includes seven figures and can be found with this article at http://dx.doi.org/10.1016/j.molcel.2017.07.024.

AUTHOR CONTRIBUTIONS

W.L. and H.S. designed the experiments. H.S., F.Y., and Q.W. performed the experiments. Q.S., J.H., and Y.Z. constructed the plasmids. C.P. and C.C.L.W. performed the mass spectrometry. W.L. and H.S. wrote the manuscript. All authors discussed the results and commented on the manuscript.

ACKNOWLEDGMENTS

We thank Dr. Q.Y. Lei for sharing PCAF and GCN5 plasmids, Dr. S.C. Lin for TIP60 plasmid, Dr. Z.P. Xia for AMPKα1/α2 double-knockout MEFs, Dr. H. Shen for *TSC2*$^{-/-}$ MEFs, and Dr. Y.S. Zhu for *ULK1*$^{-/-}$ MEFs. This study was supported by the National Natural Science Foundation of China (31530040, 31671434, and 31271431) and the National Basic Research Program of China (2013CB910200).

Received: May 2, 2017
Revised: June 13, 2017
Accepted: July 26, 2017
Published: August 24, 2017

REFERENCES

Asara, J.M., Christofk, H.R., Freimark, L.M., and Cantley, L.C. (2008). A label-free quantification method by MS/MS TIC compared to SILAC and spectral counting in a proteomics screen. Proteomics *8*, 994–999.

Axe, E.L., Walker, S.A., Manifava, M., Chandra, P., Roderick, H.L., Habermann, A., Griffiths, G., and Ktistakis, N.T. (2008). Autophagosome formation from membrane compartments enriched in phosphatidylinositol 3-phosphate and dynamically connected to the endoplasmic reticulum. J. Cell Biol. *182*, 685–701.

Backer, J.M. (2008). The regulation and function of Class III PI3Ks: novel roles for Vps34. Biochem. J. *410*, 1–17.

Bánréti, A., Sass, M., and Graba, Y. (2013). The emerging role of acetylation in the regulation of autophagy. Autophagy *9*, 819–829.

Bordoli, L., Hüsser, S., Lüthi, U., Netsch, M., Osmani, H., and Eckner, R. (2001). Functional analysis of the p300 acetyltransferase domain: the PHD finger of p300 but not of CBP is dispensable for enzymatic activity. Nucleic Acids Res. *29*, 4462–4471.

Burke, J.E., Perisic, O., Masson, G.R., Vadas, O., and Williams, R.L. (2012). Oncogenic mutations mimic and enhance dynamic events in the natural activation of phosphoinositide 3-kinase p110α (PIK3CA). Proc. Natl. Acad. Sci. USA *109*, 15259–15264.

Cantó, C., Gerhart-Hines, Z., Feige, J.N., Lagouge, M., Noriega, L., Milne, J.C., Elliott, P.J., Puigserver, P., and Auwerx, J. (2009). AMPK regulates energy expenditure by modulating NAD^+ metabolism and SIRT1 activity. Nature *458*, 1056–1060.

Chang, C., Su, H., Zhang, D., Wang, Y., Shen, Q., Liu, B., Huang, R., Zhou, T., Peng, C., Wong, C.C.L., et al. (2015). AMPK-dependent phosphorylation of GAPDH triggers Sirt1 activation and is necessary for autophagy upon glucose starvation. Mol. Cell *60*, 930–940.

Cheng, X., Ma, X., Ding, X., Li, L., Jiang, X., Shen, Z., Chen, S., Liu, W., Gong, W., and Sun, Q. (2017). Pacer mediates the function of Class III PI3K and HOPS complexes in autophagosome maturation by engaging Stx17. Mol. Cell *65*, 1029–1043.e5.

Cheong, H., Lindsten, T., Wu, J., Lu, C., and Thompson, C.B. (2011). Ammonia-induced autophagy is independent of ULK1/ULK2 kinases. Proc. Natl. Acad. Sci. USA *108*, 11121–11126.

Codogno, P., Mehrpour, M., and Proikas-Cezanne, T. (2011). Canonical and non-canonical autophagy: variations on a common theme of self-eating? Nat. Rev. Mol. Cell Biol. *13*, 7–12.

Eng, C.H., Yu, K., Lucas, J., White, E., and Abraham, R.T. (2010). Ammonia derived from glutaminolysis is a diffusible regulator of autophagy. Sci. Signal. *3*, ra31.

Fujita, N., Itoh, T., Omori, H., Fukuda, M., Noda, T., and Yoshimori, T. (2008). The Atg16L complex specifies the site of LC3 lipidation for membrane biogenesis in autophagy. Mol. Biol. Cell *19*, 2092–2100.

Grotemeier, A., Alers, S., Pfisterer, S.G., Paasch, F., Daubrawa, M., Dieterle, A., Viollet, B., Wesselborg, S., Proikas-Cezanne, T., and Stork, B. (2010). AMPK-independent induction of autophagy by cytosolic Ca^{2+} increase. Cell. Signal. *22*, 914–925.

Huang, R., Xu, Y., Wan, W., Shou, X., Qian, J., You, Z., Liu, B., Chang, C., Zhou, T., Lippincott-Schwartz, J., and Liu, W. (2015). Deacetylation of nuclear LC3 drives autophagy initiation under starvation. Mol. Cell *57*, 456–466.

Ichimura, Y., Kirisako, T., Takao, T., Satomi, Y., Shimonishi, Y., Ishihara, N., Mizushima, N., Tanida, I., Kominami, E., Ohsumi, M., et al. (2000). A ubiquitin-like system mediates protein lipidation. Nature *408*, 488–492.

Figure 7. p300-mediated VPS34 Acetylation in Mouse Liver Autophagy and in LD Breakdown in Hepatocytes

(A) Representative LC3 immunostaining in mouse liver tissues. The mice were subjected to starvation, or starvation with intraperitoneal CTB injection, or intraperitoneal C646 injection only. Scale bar, 10 μm.

(B) p62 protein levels in mouse liver tissues treated as in (A). Homogenates were prepared from three independent mice.

(C) Acetylation of VPS34 and p300 in mouse liver tissues treated as in (A). Homogenates were prepared from three independent mice.

(D) TEM images of autophagic vacuoles in mouse liver tissues. Mice were intraperitoneally injected with Flag-tagged rAAV-WT, rAAV-3KR, or rAAV-3KQ and were starved for 24 hr. Arrows indicate formed autophagosomes or autolysosomes. Asterisks indicates LD. Scale bar, 0.5 μm.

(E) Statistical analysis of cytoplasmic occupancy of autophagic vacuoles in (D). Data are shown as mean ± SEM, n = 30. ***$p < 0.001$.

(F) p62 protein levels in mouse liver tissues treated as in (D). Homogenates were prepared from three independent mice.

(G) Confocal images of L02 cells treated with C646, or serum-free medium for 24 hr with or without CTB. Green, BODIPY 493/503; blue, DAPI (nuclei). Scale bar, 10 μm.

(H) Confocal images of LD in serum-starved L02 cells with or without transfection of Flag-tagged VPS34 or VPS34 mutants. Green, BODIPY 493/503; red, Flag-tagged VPS34 or VPS34 mutants; blue, DAPI. Scale bar, 10 μm.

(I) Schematic model for p300-mediated VPS34 acetylation in autophagy initiation. Autophagic stimuli cause p300 inactivation and consequent VPS34 deacetylation. When deacetylation at K29 facilitates the formation of VPS34-Beclin 1 core complex, deacetylation at K771 and K781 directly enhances the interaction of VPS34 with PI, playing a critical role in VPS34 activation and autophagy initiation.

Itakura, E., Kishi, C., Inoue, K., and Mizushima, N. (2008). Beclin 1 forms two distinct phosphatidylinositol 3-kinase complexes with mammalian Atg14 and UVRAG. Mol. Biol. Cell *19*, 5360–5372.

Kabeya, Y., Mizushima, N., Yamamoto, A., Oshitani-Okamoto, S., Ohsumi, Y., and Yoshimori, T. (2004). LC3, GABARAP and GATE16 localize to autophagosomal membrane depending on form-II formation. J. Cell Sci. *117*, 2805–2812.

Karanam, B., Jiang, L., Wang, L., Kelleher, N.L., and Cole, P.A. (2006). Kinetic and mass spectrometric analysis of p300 histone acetyltransferase domain autoacetylation. J. Biol. Chem. *281*, 40292–40301.

Kihara, A., Noda, T., Ishihara, N., and Ohsumi, Y. (2001). Two distinct Vps34 phosphatidylinositol 3-kinase complexes function in autophagy and carboxypeptidase Y sorting in Saccharomyces cerevisiae. J. Cell Biol. *152*, 519–530.

Kim, J., Kundu, M., Viollet, B., and Guan, K.L. (2011). AMPK and mTOR regulate autophagy through direct phosphorylation of Ulk1. Nat. Cell Biol. *13*, 132–141.

Kim, J., Kim, Y.C., Fang, C., Russell, R.C., Kim, J.H., Fan, W., Liu, R., Zhong, Q., and Guan, K.L. (2013). Differential regulation of distinct Vps34 complexes by AMPK in nutrient stress and autophagy. Cell *152*, 290–303.

Lee, I.H., and Finkel, T. (2009). Regulation of autophagy by the p300 acetyltransferase. J. Biol. Chem. *284*, 6322–6328.

Lee, I.H., Cao, L., Mostoslavsky, R., Lombard, D.B., Liu, J., Bruns, N.E., Tsokos, M., Alt, F.W., and Finkel, T. (2008). A role for the NAD-dependent deacetylase Sirt1 in the regulation of autophagy. Proc. Natl. Acad. Sci. USA *105*, 3374–3379.

Liang, C., Feng, P., Ku, B., Dotan, I., Canaani, D., Oh, B.H., and Jung, J.U. (2006). Autophagic and tumour suppressor activity of a novel Beclin1-binding protein UVRAG. Nat. Cell Biol. *8*, 688–699.

Lin, S.Y., Li, T.Y., Liu, Q., Zhang, C., Li, X., Chen, Y., Zhang, S.M., Lian, G., Liu, Q., Ruan, K., et al. (2012). GSK3-TIP60-ULK1 signaling pathway links growth factor deprivation to autophagy. Science *336*, 477–481.

Lipinski, M.M., Hoffman, G., Ng, A., Zhou, W., Py, B.F., Hsu, E., Liu, X., Eisenberg, J., Liu, J., Blenis, J., et al. (2010). A genome-wide siRNA screen reveals multiple mTORC1 independent signaling pathways regulating autophagy under normal nutritional conditions. Dev. Cell *18*, 1041–1052.

Luhr, M., Szalai, P., Sætre, F., Gerner, L., Seglen, P.O., and Engedal, N. (2017). A simple cargo sequestration assay for quantitative measurement of nonselective autophagy in cultured cells. Methods Enzymol. *587*, 351–364.

Mariño, G., Pietrocola, F., Eisenberg, T., Kong, Y., Malik, S.A., Andryushkova, A., Schroeder, S., Pendl, T., Harger, A., Niso-Santano, M., et al. (2014). Regulation of autophagy by cytosolic acetyl-coenzyme A. Mol. Cell *53*, 710–725.

Matsunaga, K., Saitoh, T., Tabata, K., Omori, H., Satoh, T., Kurotori, N., Maejima, I., Shirahama-Noda, K., Ichimura, T., Isobe, T., et al. (2009). Two Beclin 1-binding proteins, Atg14L and Rubicon, reciprocally regulate autophagy at different stages. Nat. Cell Biol. *11*, 385–396.

Matsunaga, K., Morita, E., Saitoh, T., Akira, S., Ktistakis, N.T., Izumi, T., Noda, T., and Yoshimori, T. (2010). Autophagy requires endoplasmic reticulum targeting of the PI3-kinase complex via Atg14L. J. Cell Biol. *190*, 511–521.

McKnight, N.C., Zhong, Y., Wold, M.S., Gong, S., Phillips, G.R., Dou, Z., Zhao, Y., Heintz, N., Zong, W.X., and Yue, Z. (2014). Beclin 1 is required for neuron viability and regulates endosome pathways via the UVRAG-VPS34 complex. PLoS Genet. *10*, e1004626.

Miller, S., Tavshanjian, B., Oleksy, A., Perisic, O., Houseman, B.T., Shokat, K.M., and Williams, R.L. (2010). Shaping development of autophagy inhibitors with the structure of the lipid kinase Vps34. Science *327*, 1638–1642.

Mizushima, N., Yamamoto, A., Matsui, M., Yoshimori, T., and Ohsumi, Y. (2004). In vivo analysis of autophagy in response to nutrient starvation using transgenic mice expressing a fluorescent autophagosome marker. Mol. Biol. Cell *15*, 1101–1111.

Nishimura, T., Kaizuka, T., Cadwell, K., Sahani, M.H., Saitoh, T., Akira, S., Virgin, H.W., and Mizushima, N. (2013). FIP200 regulates targeting of Atg16L1 to the isolation membrane. EMBO Rep. *14*, 284–291.

Pietrocola, F., Lachkar, S., Enot, D.P., Niso-Santano, M., Bravo-San Pedro, J.M., Sica, V., Izzo, V., Maiuri, M.C., Madeo, F., Mariño, G., and Kroemer, G. (2015a). Spermidine induces autophagy by inhibiting the acetyltransferase EP300. Cell Death Differ. *22*, 509–516.

Pietrocola, F., Galluzzi, L., Bravo-San Pedro, J.M., Madeo, F., and Kroemer, G. (2015b). Acetyl coenzyme A: a central metabolite and second messenger. Cell Metab. *21*, 805–821.

Rudge, S.A., Anderson, D.M., and Emr, S.D. (2004). Vacuole size control: regulation of PtdIns(3,5)P_2 levels by the vacuole-associated Vac14-Fig4 complex, a PtdIns(3,5)P_2-specific phosphatase. Mol. Biol. Cell *15*, 24–36.

Russell, R.C., Tian, Y., Yuan, H., Park, H.W., Chang, Y.Y., Kim, J., Kim, H., Neufeld, T.P., Dillin, A., and Guan, K.L. (2013). ULK1 induces autophagy by phosphorylating Beclin-1 and activating VPS34 lipid kinase. Nat. Cell Biol. *15*, 741–750.

Scarlatti, F., Maffei, R., Beau, I., Codogno, P., and Ghidoni, R. (2008). Role of non-canonical Beclin 1-independent autophagy in cell death induced by resveratrol in human breast cancer cells. Cell Death Differ. *15*, 1318–1329.

Sebti, S., Prébois, C., Pérez-Gracia, E., Bauvy, C., Desmots, F., Pirot, N., Gongora, C., Bach, A.S., Hubberstey, A.V., Palissot, V., et al. (2014). BAT3 modulates p300-dependent acetylation of p53 and autophagy-related protein 7 (ATG7) during autophagy. Proc. Natl. Acad. Sci. USA *111*, 4115–4120.

Shi, D., Pop, M.S., Kulikov, R., Love, I.M., Kung, A.L., and Grossman, S.R. (2009). CBP and p300 are cytoplasmic E4 polyubiquitin ligases for p53. Proc. Natl. Acad. Sci. USA *106*, 16275–16280.

Smith, D.M., Patel, S., Raffoul, F., Haller, E., Mills, G.B., and Nanjundan, M. (2010). Arsenic trioxide induces a beclin-1-independent autophagic pathway via modulation of SnoN/SkiL expression in ovarian carcinoma cells. Cell Death Differ. *17*, 1867–1881.

Sun, Q., Zhang, J., Fan, W., Wong, K.N., Ding, X., Chen, S., and Zhong, Q. (2011). The RUN domain of rubicon is important for hVps34 binding, lipid kinase inhibition, and autophagy suppression. J. Biol. Chem. *286*, 185–191.

Sun, T., Li, X., Zhang, P., Chen, W.D., Zhang, H.L., Li, D.D., Deng, R., Qian, X.J., Jiao, L., Ji, J., et al. (2015). Acetylation of Beclin 1 inhibits autophagosome maturation and promotes tumour growth. Nat. Commun. *6*, 7215.

Taguchi-Atarashi, N., Hamasaki, M., Matsunaga, K., Omori, H., Ktistakis, N.T., Yoshimori, T., and Noda, T. (2010). Modulation of local PtdIns3P levels by the PI phosphatase MTMR3 regulates constitutive autophagy. Traffic *11*, 468–478.

Thompson, P.R., Wang, D., Wang, L., Fulco, M., Pediconi, N., Zhang, D., An, W., Ge, Q., Roeder, R.G., Wong, J., et al. (2004). Regulation of the p300 HAT domain via a novel activation loop. Nat. Struct. Mol. Biol. *11*, 308–315.

Tian, S., Lin, J., Jun Zhou, J., Wang, X., Li, Y., Ren, X., Yu, W., Zhong, W., Xiao, J., Sheng, F., et al. (2010). Beclin 1-independent autophagy induced by a Bcl-X_L/Bcl-2 targeting compound, Z18. Autophagy *6*, 1032–1041.

Vicinanza, M., Korolchuk, V.I., Ashkenazi, A., Puri, C., Menzies, F.M., Clarke, J.H., and Rubinsztein, D.C. (2015). PI(5)P regulates autophagosome biogenesis. Mol. Cell *57*, 219–234.

Yamamoto, A., Cremona, M.L., and Rothman, J.E. (2006). Autophagy-mediated clearance of huntingtin aggregates triggered by the insulin-signaling pathway. J. Cell Biol. *172*, 719–731.

Yang, W., Hong, Y.H., Shen, X.Q., Frankowski, C., Camp, H.S., and Leff, T. (2001). Regulation of transcription by AMP-activated protein kinase: phosphorylation of p300 blocks its interaction with nuclear receptors. J. Biol. Chem. *276*, 38341–38344.

Yang, Y., Fiskus, W., Yong, B., Atadja, P., Takahashi, Y., Pandita, T.K., Wang, H.G., and Bhalla, K.N. (2013). Acetylated hsp70 and KAP1-mediated Vps34 SUMOylation is required for autophagosome creation in autophagy. Proc. Natl. Acad. Sci. USA *110*, 6841–6846.

Zhang, Y., Qiu, J., Wang, X., Zhang, Y., and Xia, M. (2011). AMP-activated protein kinase suppresses endothelial cell inflammation through phosphorylation of transcriptional coactivator p300. Arterioscler. Thromb. Vasc. Biol. *31*, 2897–2908.

Zhang, T., Dong, K., Liang, W., Xu, D., Xia, H., Geng, J., Najafov, A., Liu, M., Li, Y., Han, X., et al. (2015). G-protein-coupled receptors regulate autophagy by ZBTB16-mediated ubiquitination and proteasomal degradation of Atg14L. eLife *4*, e06734.

Zhong, Y., Wang, Q.J., Li, X., Yan, Y., Backer, J.M., Chait, B.T., Heintz, N., and Yue, Z. (2009). Distinct regulation of autophagic activity by Atg14L and Rubicon associated with Beclin 1-phosphatidylinositol-3-kinase complex. Nat. Cell Biol. *11*, 468–476.

Zhu, J.H., Horbinski, C., Guo, F., Watkins, S., Uchiyama, Y., and Chu, C.T. (2007). Regulation of autophagy by extracellular signal-regulated protein kinases during 1-methyl-4-phenylpyridinium-induced cell death. Am. J. Pathol. *170*, 75–86.

STAR★METHODS

KEY RESOURCES TABLE

REAGENT or RESOURCE	SOURCE	IDENTIFIER
Antibodies		
Rabbit polyclonal anti-p300	Santa Cruz Biotechnology	Cat#sc-585
Rabbit polyclonal anti-HA	Santa Cruz Biotechnology	Cat#sc-805
Mouse monoclonal anti-HA	Santa Cruz Biotechnology	Cat#sc-7392
Mouse monoclonal anti-Myc	Santa Cruz Biotechnology	Cat#sc-40
Rabbit polyclonal anti-GST	Santa Cruz Biotechnology	Cat#sc-459
Mouse monoclonal anti-Flag	Santa Cruz Biotechnology	Cat#sc-51590
Rabbit polyclonal anti-Flag	Santa Cruz Biotechnology	Cat#sc-807
Mouse monoclonal anti-Lamp1	Santa Cruz Biotechnology	Cat#sc-20011
Rabbit polyclonal anti-Lamin B1	Santa Cruz Biotechnology	Cat#sc-20682
Rabbit polyclonal anti-LC3B	Sigma	Cat#L7543
Mouse monoclonal anti-β-Actin	Sigma	Cat#A5316
Mouse monoclonal anti-α-Tubulin	Sigma	Cat#T8203
Rabbit polyclonal anti-ATG14L	Cell Signaling Technology	Cat#5504
Rabbit polyclonal anti-VPS34	Cell Signaling Technology	Cat#3811
Rabbit polyclonal anti-VPS34 for IP	Echelon Biosciences	Cat#Z-R015
Rabbit polyclonal anti-histone H3	Cell Signaling Technology	Cat#9715
Rabbit polyclonal anti-acetyl-histone H3(Lys56)	Cell Signaling Technology	Cat#4243
Rabbit polyclonal anti-acetylated-lysine	Cell Signaling Technology	Cat#9441
Rabbit polyclonal anti-acetyl-CBP(Lys1535)/p300(Lys1499)	Cell Signaling Technology	Cat#4771
Rabbit polyclonal anti-p150	Cell Signaling Technology	Cat#14580
Mouse monoclonal anti-Beclin 1	Cell Signaling Technology	Cat#4122
Rabbit monoclonal anti-UVRAG	Cell Signaling Technology	Cat#13115
Rabbit polyclonal anti-Beclin 1	Proteintech	Cat#11306-1-AP
Rabbit polyclonal anti-p62/SQSTM1	Proteintech	Cat#18420-1-AP
Rabbit polyclonal anti-GFP	Proteintech	Cat#50430-2-AP
Mouse monoclonal anti-LC3	Cosmo Bio	Cat#CAC-CTB-LC3-2-I
Mouse monoclonal anti-ATG14L	ABGENT	Cat#AO2189a
Donkey ploYclonal anti-mouse IgG-HRP	Santa Cruz Biotechnology	Cat#sc-2314
Donkey ploYclonal anti-rabbit IgG-HRP	Santa Cruz Biotechnology	Cat#sc-2313
Donkey anti-rabbit IgG (H+L) IRDye800CW	LI-COR Biosciences	Cat#926-32213
Donkey anti-mouse IgG (H+L) IRDye680RD	LI-COR Biosciences	Cat#926-68072
Glutathione-Sepharose 4B beads	GE Healthcare Life Sciences	Cat#17-0756-01
Protein G PLUS-Agarose	Santa Cruz Biotechnology	Cat#sc-2002
Protein A Agarose	Santa Cruz Biotechnology	Cat#sc-2001
Goat anti-Mouse IgG (H+L), Alexa Fluor 488	Molecular Probes	Cat#A-11001
Donkey anti-Rabbit IgG (H+L), Alexa Fluor 488	Molecular Probes	Cat#A-21206
Goat anti-Rabbit IgG (H+L), Alexa Fluor 546	Molecular Probes	Cat#A-11081
Donkey anti-Mouse IgG (H+L), Alexa Fluor 546	Molecular Probes	Cat#A10036
BODIPY 493/503	Invitrogen	Cat#D3922
DAPI	Beyotime	Cat#C1002

(*Continued on next page*)

Continued

REAGENT or RESOURCE	SOURCE	IDENTIFIER
anti-HA affinity beads	Biotool	Cat#B23302
Rabbit ploYclonal anti-Rubicon	Abcam	Cat#ab92388
Rabbit monoclonal anti-ATG7	Abcam	Cat#ab133528
Rabbit ploYclonal anti-Rab5	Abcam	Cat#ab18211
Mouse monoclonal anti-Rab7	Abcam	Cat#ab50533
Rabbit monoclonal anti-EGFR	Abcam	Cat#ab52894
Mouse monoclonal anti-ATG5	MBL	Cat#M153-3
Bacterial and Virus Strains		
E. coli BL21	Transgen Biotech	Cat#CD601
Trans 5α	Transgen Biotech	Cat#CD201
Chemicals, Peptides, and Recombinant Proteins		
Trichostatin A	Sigma-Aldrich	Cat#T1952
Nicotinamide	Sigma-Aldrich	Cat#72340
CTB	Sigma-Aldrich	Cat#C6499
C646	Selleck	Cat#S7152
γ-^{32}P-ATP	PerkinElmer	Cat#NEG502A
3-methyladenine (3-MA)	Sigma-Aldrich	Cat#M9281
Torin1	Selleck	Cat#S2827
Tissue-Tek OCT compound	Sakura	Cat#4583
Cocktail	Roche	Cat#04693132001
DPDPB (1,4-bis(3-(2-pyridyldithio) propionamido butane)	Sigma-Aldrich	Cat#16646
Acetyl-coenzyme A	Sigma-Aldrich	Cat#A2056
Glucose-free DMEM	Life Technologies	Cat#11966025
Lipofectamine 2000	Invitrogen	Cat#11668019
UK5099 (2-Cyano-3-(1-phenyl-1H-indol-3-yl)−2-propenoic acid)	Sigma	Cat#PZ0160
Dichloroacetate (DCA)	Sigma	Cat#347795
I-CBP112	Sigma	Cat#SML1134
SGC-CBP30	Selleck	Cat#S7256
p300-HAT	Upstate	Cat#14-418
Critical Commercial Assays		
BCA protein assay kit	Thermo	Cat#23227
PicoProbe Acetyl CoA Assay Kit (Fluorometric)	Abcam	Cat#ab87546
Class III PI3-Kinase ELISA Assay Kit	Echelon	Cat#K-3000
Deposited Data		
Original images were deposited to Mendeley data	This paper	http://dx.doi.org/10.17632/x3tsv9hjx3.1
Experimental Models: Cell Lines		
HEK293	ATCC	ATCC CRL-1573
HEK293T	ATCC	ATCC CRL-3216
HeLa	ATCC	ATCC CCL-2
L02	Laboratory of Qiming Sun	N/A
TSC2$^{-/-}$ MEFs	Laboratory of Han-Ming Shen	N/A
ULK1$^{-/-}$ MEFs	Laboratory of Yushan Zhu	N/A
AMPK$^{-/-}$ MEF	Laboratory of Zongping Xia	N/A
FIP200$^{-/-}$ MEF	Laboratory of Han-Ming Shen	N/A

(*Continued on next page*)

Continued

REAGENT or RESOURCE	SOURCE	IDENTIFIER
GFP-LC3 HEK293	Chang et al., 2015	N/A
p300-KO HEK293	Constructed in our lab	N/A
Beclin 1-KO HEK293	Constructed in our lab	N/A
Experimental Models: Organisms/Strains		
Female C57BL/6 mice	Vital River, Beijing, China	N/A
Oligonucleotides		
p300 siRNA: CUAGAGACACCUUGUAGUATT	This paper	N/A
VPS34 siRNA: CCCAUGAGAUGUACUUGAACGUAAU	This paper	N/A
Non-targeting siRNA: UUCUCCGAACGUGUCACGUTT	This paper	N/A
Recombinant DNA		
VPS34-29R771R781R-Flag plasmid	This paper	N/A
VPS34-29Q771Q781Q-Flag plasmid	This paper	N/A
VPS34-29Q-Flag plasmid	This paper	N/A
VPS34-29R-Flag plasmid	This paper	N/A
VPS34-771R-Flag plasmid	This paper	N/A
VPS34-771Q-Flag plasmid	This paper	N/A
VPS34-781R-Flag plasmid	This paper	N/A
VPS34-781Q-Flag plasmid	This paper	N/A
VPS34-29Q771R781R-Flag plasmid	This paper	N/A
VPS34-29R771Q781Q-Flag plasmid	This paper	N/A
GST- VPS34-29Q771Q781Q plasmid	This paper	N/A
GST- VPS34-29Q plasmid	This paper	N/A
GST- VPS34-771R plasmid	This paper	N/A
GST- VPS34-771Q plasmid	This paper	N/A
GST- VPS34-781Q plasmid	This paper	N/A
pXF4H-p150-HA plasmid	This paper	N/A
pEP-p300-KO plasmid	This paper	N/A
pEP-Beclin 1-KO plasmid	This paper	N/A
Myc-GCN5 plasmid	Laboratory of Qunying Lei	N/A
Flag-PCAF plasmid	Laboratory of Qunying Lei	N/A
Myc-TIP60 plasmid	Laboratory of Shengcai Lin	N/A
CBP-HA plasmid	Laboratory of Jimin Shao	N/A
p300-HA plasmid	Laboratory of Jimin Shao	N/A
Software and Algorithms		
Odyssey infrared imaging system	LI-COR Biosciences	N/A
DNA STAR sequence assay	http://www.dnastar.com	N/A
LSM 510 software	Zeiss	N/A
GraphPad Prism software	GraphPad Software Inc	http://www.graphpad.com
Other		
All restriction enzyme	Thermo Fisher Scientific	
QuikChange II XL	Stratagene	Cat#200518
KOD-plus-neo	TOYOBO	KOD-401

CONTACT FOR REAGENT AND RESOURCE SHARING

Further information and requests for resources and reagents should be directed to and will be fulfilled by the Lead Contact, Wei Liu (liuwei666@zju.edu.cn).

EXPERIMENTAL MODEL AND SUBJECT DETAILS

Cell culture

Unless otherwise stated, HEK293 cells were used. HEK293, HEK293T, L02 and mouse embryonic fibroblasts (MEFs) were cultured in DMEM supplemented with 10% FBS in a 37°C incubator with a humidified, 5% CO_2 atmosphere. For amino acid starvation, cells were washed three times with PBS and incubated in amino-acid-free medium supplemented with 10% dialyzed FBS for 4 hr. For glucose starvation, cells were washed three times with PBS and incubated in glucose-free DMEM containing 10% dialyzed FBS for 4 hr.

Stable cell lines construction

pEP-p300-KO plasmid was made by cloning the target DNA sequence of human p300 (TAGTTCCCCTAACCTCAATA) into a pEP-KO Z1779 vector using Sap I. p300-KO HEK293 cells were created by transient transfection of pEP-p300-KO plasmid followed by selection with 1.25 μg/ml puromycin. pEP-Beclin 1-KO plasmid was made by cloning the target DNA sequence of human Beclin 1 (TCCTGGTTTCGCCTGGGCTG) into a pEP-KO Z1779 vector using Sap I. Beclin 1-KO HEK293 cells were created by transient transfection of pEP-Beclin 1-KO plasmid followed by selection with 1.25 μg/ml puromycin.

Mice feeding

Female C57BL/6 mice aged 7 weeks were housed in a temperature-controlled environment under a 12 hr light/dark cycle and received food and water ad libitum. Mouse experiments were approved by the Review Committee of Zhejiang University School of Medicine.

METHOD DETAILS

Reagents

Unless otherwise stated, the chemicals were used as follows: Trichostatin A (400 nM) were added to the cultural medium for 16 hr. Nicotinamide (5 mM) was added to the medium for 8 hr. CTB (50 μM) was added to the medium 4 hr before cell starvation or NH_4Cl treatment, or in separate treatment for 6 hr. C646 (10 μM) were added to the medium for 4 hr. I-CBP112 (5 μM) or SGC-CBP30 (2.5 μM) was added to the medium for 6 hr. UK5099 (20 μM) or DCA (20 mM) was added to the medium for 20 hr. Chloroquine (50 μM) was added to the medium 30 min before amino acid- or glucose-starvation or SGC-CBP30 treatment. 3-methyladenine (3-MA) was either added to the medium for 2 hr (10 mM) after 2 hr C646 treatment or was added to the lipid kinase reaction (5 mM). NH_4Cl (2 mM) was added to cultural medium for 16 hr. Torin1 (200 nM) was added to the medium for 4 hr.

Transfection

Transient transfection was performed using Lipofectamine 2000 according to the manufacturer's instructions. Cells were analyzed 18-24 hr after transfection.

For RNA interference, siRNA duplexes designed against conserved target sequences were transfected using Lipofectamine 2000 for 48 hr, as specified by the manufacturer.

Cell imaging

Cells were cultured on coverslips and fixed in 4% formaldehyde for 10 min at room temperature. After washing twice in PBS, cells were incubated in PBS containing 10% FBS to block nonspecific sites of antibody adsorption. The cells were then incubated with the appropriate primary antibodies (diluted 1:100) and secondary antibodies (diluted 1:500) in PBS containing 0.1% saponin and 10% FBS as indicated in the Figure legends. For LD staining, cells were incubated with BODIPY 493/503 (Invitrogen, 10 μg/ml) in PBS for 1 hr at 37°C. Confocal images were captured in multitracking mode on a Meta laser-scanning confocal microscope 510 (Carl Zeiss) with a 63 × Plan Apochromat 1.4 NA objective and analyzed with the LSM 510 software.

Tissue samples for LC3 assessment were prepared as follows. To prevent the induction of autophagy during tissue preparation, mice were anesthetized with diethylether. Fresh liver tissues were harvested and immediately frozen in liquid nitrogen. Then tissue samples were embedded in Tissue-Tek OCT compound and stored at −80°C. The samples were sectioned at 5 μm on a cryostat (CM1950, Leica). Immunostaining of LC3 was performed as described above.

Immunoblot and immunoprecipitation

Cells were harvested and lysed in RIPA buffer (50 mM Tris-HCl, pH 7.4, 150 mM NaCl, 1% Triton X-100, 1% sodium deoxycholate, 0.1% SDS, 1 mM EDTA) supplemented with complete protease inhibitor cocktail. Proteins were resolved on SDS polyacrylamide

gels, and then transferred to a polyvinylidene difluoride membrane. After blocking with 5% (w/v) bovine serum albumin, the membrane was stained with the corresponding primary antibodies. After incubation with the corresponding secondary antibodies, for cell samples, specific bands were analyzed using an Odyssey infrared imaging system (LI-COR Biosciences); for tissue samples, specific bands were analyzed by ECL (Bio-Rad) and autoradiography.

For immunoprecipitation, cells were lysed in Nonidet P-40 (NP-40) lysis buffer (20 mM Tris-HCl, pH 7.5, 1% NP-40, 137 mM NaCl, 1 mM $MgCl_2$, 1 mM $CaCl_2$, 10% glycerol, 1 mM $Na_4P_2O_7$, 1 mM Na_3VO_4, 10 mM NaF, 1 μM TSA, 5 mM NAM) supplemented with complete protease inhibitor cocktail. Then immunoprecipitation was performed using the indicated antibodies. Generally, 2 μg of antibody was added to 1 mL of cell lysate and incubated at 4°C overnight. After addition of protein A/G-agarose beads, incubation was continued for 2 hr, and then immunocomplexes were washed five times using lysis buffer, resolved by SDS-PAGE, and analyzed by immunoblot. For the analysis of p300 and VPS34 interaction, cells were treated with 100 μM cross-linker DPDPB [1,4-bis(3-(2-pyridyldithio)propionamido)butane, Sigma-Aldrich] for 1 hr on ice before lysis. Cross-linker was cut off by boiling the sample in Laemmli sample buffer containing 50 mM DTT for 10 min.

Tissue samples for immunoprecipitation were prepared as follows: liver tissues were extracted and homogenized in two cycles using TissuePreP (Gering Scientific) in RIPA buffer supplemented with complete protease inhibitor cocktail, TSA and NAM. The tissue extracts were then centrifuged at 13,000 g at 4°C and the supernatants were collected. Protein concentrations in the supernatants were measured with a BCA protein assay kit.

Recombinant protein purification and in vitro acetylation assay

GST-VPS34 was expressed in *Escherichia coli* BL21. Bacteria were treated with 0.1 mM IPTG at 23°C to induce protein expression, and were harvested and resuspended in PBS containing 0.5% Triton X-100, 2 mM EDTA, and 1 mM PMSF, followed by ultrasonication. The recombinant VPS34 proteins were purified using glutathione-Sepharose 4B beads, eluted with glutathione, and dialyzed using Slide-A-Lyzer Dialysis Cassettes (Pierce) against 20 mM Tris-HCl at pH 8.0 and 10% glycerol.

p300-HA protein was purified from HEK293T cells 48 hr after transfection by immunoprecipitation with anti-HA affinity beads (Selleck). Endogenous p300 was purified from the cytosol fraction of same number of HEK293 cells by immunoprecipitation with anti-p300. Recombinant GST-p300 HAT domain purified from *Escherichia coli* was purchased from Upstate. For in vitro acetylation assay, GST-VPS34 protein (10 μg) was incubated with purified recombinant p300 protein (1 μg), or p300-HA immunoprecipitated from cell lysate, or p300 immunoprecipitated from cell cytosol, in the presence of acetyl-coenzyme A (4 μg) and 10 μL 5 × HAT assay buffer (250 mM Tris–HCl, pH 8.0, 50% glycerol, 0.5 mM EDTA, 5 mM dithiothreitol) in a total volume of 50 μl. The contents were mixed gently and placed in a 30°C shaking incubator for 4 hr. Then 2 × protein loading buffer (50 μl) was added to the reaction and the mixture was boiled for 5 min. The reaction products were separated by SDS-PAGE and immunoblotted with anti-acetyl-lysine.

Subcellular fractionation

HEK293 Cells were treated with or without SGC-CBP30 for 6 hr. The cells were washed with PBS and scraped into hypotonic buffer (10 mM HEPES, pH 7.4, 10 mM KCl, 1.5 mM $MgCl_2$, 0.5 mM DTT). The suspension was put on ice for 30 min to allow swelling. The cells were then Dounce-homogenized (20-30 strokes) with a tight-fitting pestle. After centrifugation at 500 g for 5 min at 4°C, the supernatant was used as the cytoplasmic fraction. The pellet was washed twice with hypotonic buffer and reconstituted in 0.5% NP-40 lysis buffer. After centrifugation at 15,000 g for 30 min, the resultant supernatant was used as the nuclear fraction. All buffers used throughout processing contained protease inhibitors and deacetylase inhibitors.

Fluorometric acetyl-CoA quantitation assay

Intracellular acetyl-CoA levels in UK5099- or DCA-treated cells were measured using the PicoProbe Acetyl CoA Assay Kit (Abcam) according to the manufacturer's instructions. Briefly, HeLa cells were treated with UK5099 (20 μM) or DCA (20 mM) for 20 hr and then harvested and sonicated. After centrifugation at 15,000 g for 15 min at 4°C to remove the insoluble materials, the samples were deproteinized by perchloric acid precipitation and incubated with Reaction Mix (acetyl-CoA substrates, conversion enzyme mix, and fluorescent probe detector) at 37°C for 10 min. The intracellular acetyl-CoA level was assessed by measuring the fluorescent emission at 587 nm following excitation at 535 nm. After correcting the background from all readings, values for each sample were determined and normalized by protein concentration of each sample.

HPLC-MS/MS

To identify the acetylation site of VPS34 or quantified VPS34 acetylation degree by mass spectrometry, the gel band of acetylated GST-VPS34 or cellular VPS34 was excised. In-gel digestion of VPS34 was performed with grade modified trypsin (Promega) at 37°C overnight. The digested peptides were desalted and loaded on a capillary reverse-phase C18 column packed in-house (15 cm in length, 100 μm ID × 360 μm OD, 3 μm particle size, 100 Å pore diameter) connected to an Easy LC 1000 system. The samples were analyzed with a 180 min HPLC gradient from 0% to 100% buffer B (buffer A: 0.1% formic acid in water; buffer B: 0.1% formic acid in acetonitrile) at 300 nL/min. The eluted peptides were ionized and directly introduced into a Q-Exactive or Fusion mass spectrometer (Thermo) using a nano-spray source. Survey full-scan MS spectra (m/z 300-1800) were acquired in the Orbitrap analyzer with resolution r = 70,000 at m/z 400.

Analysis of tandem mass spectra

Protein identification and post-translational modification analysis were done with Integrated Proteomics Pipeline-IP2 (Integrated Proteomics Applications, Inc., http://www.integratedproteomics.com) using ProLuCID/Sequest, DTASelect2. Spectrum raw files were extracted into ms2 files from raw files using RawExtract, and the tandem mass spectra were searched against the Uniprot human protein database, plus sequences of known contaminants such as keratin and porcine trypsin concatenated to a decoy database in which the sequence for each entry in the original database was reversed using ProLuCID/Sequest. Carbamidomethylation (+57.02146) of cysteine was considered as a static modification. Methionine oxidation and lysine acetylation were set as variable modifications. The search space included all fully- and half-tryptic peptide candidates with missed cleavage restrictions. The ProLuCID search results were assembled and filtered using the DTASelect program (version 2.0) with a false discovery rate of 0.01; under such conditions, the estimated false discovery rate was below ~1% at the protein level in all analyses.

To quantify the degree of acetylation at the specific sites in VPS34, we used the spectral counting approach (Asara et al., 2008). The stoichiometry of VPS34 acetylation was calculated by the ratio of the spectrum counts of total acetylated peptides (at K29, K771 or K781) or acetylated peptides with acetylation at each of the specific sites to total spectrum counts from three independent experiments.

In vitro VPS34 lipid kinase assay

Endogenous VPS34 and Flag-tagged VPS34 proteins were immunoprecipitated from HEK293 or HEK293T cells treated as described in the Figure legends. The immune complexes were washed three times in NP-40 lysis buffer, followed by two washes in washing buffer (100 mM Tris-HCl at pH 7.4 and 500 mM LiCl) and two washes in kinase buffer (50 mM Tris-HCl at pH 7.4, 10 mM $MgCl_2$) and pre-incubated for 10 min in 45 μL of reaction buffer (10 mM $MnCl_2$ in reaction buffer) containing 2 μg of sonicated PI. The reaction was initiated by the addition of 5 μL of ATP mix [1 μL 10 mM unlabelled ATP, 1 μL (10 μCi) γ-^{32}P-ATP, and 3 μL H_2O] and incubated for 30 min at room temperature. The reaction was terminated by adding 100 μL of 1 M HCl, extracted with 160 μL $CHCl_3$:MeOH (1:1), washed twice with MeOH:1 M HCl (1:1), dried with SpeedVac, and re-suspended in 20 μL $CHCl_3$:MeOH (1:1). Extracted phospholipid products were separated by thin-layer-chromatography using a dried coated silica gel with running buffer ($CHCl_3$:MeOH:NH_4OH:H_2O, 45:35:1.5:8.5). Plates were dried and exposed by autoradiography to visualize PI3P production.

In vitro PI3P ELISA assay

Endogenous VPS34 protein was immunoprecipitated from HeLa cells treated with UK5099 or DCA and subjected to VPS34 activity assay using Class III PI3K ELISA Kit (Echelon) following the manufacturer. Briefly, 40 μL kinase reaction buffer (50 mM Tris-HCl at pH 7.4, 10 mM $MgCl_2$, 10 mM $MnCl_2$), 8 μL of 500 μM PI, 2 μL of 1.25 mM ATP were added to the immune complex and incubated at 30°C for 1 hr. The reaction was terminated by adding 10 μL of 100 mM EDTA. The quenched reaction mixture and PI3P detector protein (provided by the Kit) were added together to the PI3P-coated microplate for competitive binding to the PI3P detector protein. The amount of PI3P detector protein bound to the plate was determined through colorimetric detection of absorbance at 450 nm. The concentration of PI3P in the reaction mixture was calculated as reversed to the amount of PI3P detector protein bound to the plate.

Liposome preparation and liposome sedimentation assay

Liposomes were composed of bovine liver PI, DOPC, and DOPE (Avanti Polar Lipids). Lipids dissolved in chloroform were mixed in a glass vial with 60% PI:25% PE:15% PC. Chloroform was evaporated under a stream of N_2 for 30 min. Lipids were further dried overnight in Concentrator Plus (Millipore). The lipid film was resuspended in 50 mM Na_2HPO_4/NaH_2PO_4 (pH 7.4). Following hydration, lipid vesicles were subjected to five freeze-thaw cycles in liquid N_2 and a room-temperature water bath, and then extruded with a 100 nm pore filter (Whatman).

For liposome binding assays, 100 μg of GST-VPS34 protein was incubated with 50 μg of liposomes or different amounts of liposomes (noted in the Figure 4C) in 50 mM Na_2HPO_4/NaH_2PO_4 (pH 7.4) at 25°C for 1 hr in a total volume of 80 μl. Samples were centrifuged in a Beckman Optima MAX-XP ultracentrifuge at 4°C for 60 min at 100,000 g. The pellets were washed twice with the same buffer. GST-VPS34 protein was detected by immunoblot.

Protein-lipid overlay assay

Lyophilized PI was reconstituted to 1 mM stock in a 1:1 solution of methanol and chloroform and stored at −80°C until use. The PI was diluted in a 2:1:0.8 solution of methanol:chloroform:water to five concentrations ranging between 0 and 250 μM. One-microliter aliquots of the selected dilutions (which contained 0 to 250 pmol of PI) were spotted onto nitrocellulose membranes (Amersham Pharmacia Biotech). The membranes were incubated in blocking buffer (50 mM Tris-HCl, pH 7.5, 150 mM NaCl, 0.1% Tween 20, 2 mg/ml fatty acid-free BSA) with gentle rocking for 1 hr after drying the membrane at room temperature. Then the membrane was incubated with blocking buffer containing 10 nM GST-VPS34 protein overnight at 4°C. The binding of the PI-bound proteins to the membrane was analyzed by ECL and autoradiography after incubating the membrane with anti-GST and rabbit HRP-conjugated secondary antibody.

LDH sequestration assay

Autophagic sequestration activity was measured as the transfer of the cytosolic enzyme lactate dehydrogenase (LDH) to sedimentable autophagic vacuoles (Luhr et al., 2017). Briefly, cells were washed with 800 μL of 37°C PBS/5% BSA. After centrifugation at 500 × g for 5 min at 4°C, the cells were resuspended in 400 μL ice-cold 10% sucrose and electrodisrupted by a single high-voltage pulse (800 V; 25 μF). Following dilution with 400 μL phosphate-buffered sucrose (100 mM sodium monophosphate, 2 mM dithiothreitol, 2 mM EDTA and 1.75% sucrose, pH 7.5), 600 μL of the disruptate was further diluted with 900 μL ice-cold resuspension buffer (50 mM sodium monophosphate, 1 mM EDTA, 1 mM DTT) containing 0.5% BSA and 0.01% Tween-20 and then centrifuged for 7 min at 5000 × g (MEF) or for 50 min at 18,000 × g (HEK293). The pellet and the remaining total-cell disruptate (200 μl) were freeze-thawed (−80°C). Then the pellet was dissolved in 400 μL resuspension buffer containing 1% Triton X-405, while the total-cell disruptate was diluted with 300 μL resuspension buffer containing 1.5% Triton X-405. Following a short centrifugation to eliminate cell debris (5 min at 18,000 × g), LDH enzymatic activity was measured using the LDH Activity Assay Kit (Sigma) according to the manufacturer's instructions. The amount of LDH sedimenting with the cell corpse pellet (sample value divided by 1.125) relative to the amount in the total disruptate (sample value multiplied by 2.5) is expressed as "sequestered LDH (% of total)" in the figures.

EGFR degradation assay

HeLa cells were transfected with Flag-tagged WT VPS34 or VPS34 mutants. Twenty four hours after transfection, the cells were cultured in serum-free DMEM for 12 hr. Then the cells were incubated on ice in serum-free DMEM medium containing 200 ng/ml of EGF for 15 min, followed by culturing in EGF-free medium at 37°C. At determined time points, the cells were lysed and subjected to immunoblot with EGFR antibody.

Mouse experiments and tissue processing

For fasting, mice were subjected to 24 hr food starvation with or without intraperitoneal injection of 30 mg/kg CTB every 8 hr during starvation. These mice had free access to drinking water. For C646 treatment, mice were subjected to a single intraperitoneal injection of 30 mg/kg of C646 with or without a single pre-injection of 60 mg/kg of CQ (4 hr before C646 injection) and sacrificed 6 hr later. For immunostaining and immunoprecipitation experiments, fresh liver tissues were immediately frozen in liquid nitrogen.

For investigating the role of VPS34 acetylation in regulating autophagy in vivo, recombinant adeno-associated virus vectors packing WT (rAAV-WT), or 3KR (rAAV-3KR), or 3KQ (rAAV-3KQ) and pseudoserotyped AAV9 caspid (Weizhen, Shandong, China), were produced in HEK293T cells. Mice were intraperitoneally injected with the rAAV-WT, rAAV-3KR or rAAV-3KQ. Four weeks after viral injection, the mice were starved for 24 hr and sacrificed for the analysis of autophagosome formation and p62 degradation.

Transmission electron microscopy

TEM was performed as described previously (Chang et al., 2015). Briefly, liver tissues were fixed in 2.5% glutaraldehyde in PBS overnight, and post-fixed in aqueous 1% OsO_4 for 1.5 hr followed by 2% uranyl acetate. After ethanol and acetone dehydration and embedding in polybed 812 resin (Polysciences, 025950-1), ultrathin (70 nm) sections were post-stained with 2% uranyl acetate followed by 0.3% lead citrate. Sections were imaged using a Tecnai G2 Spirit transmission electron microscope (FEI Company). For autophagic vacuole quantification, 30 micrographs were taken with systematic random sampling from each sample. The cytoplasmic volume fraction of autophagic vacuoles was estimated using MetaMorph (Universal Imaging Corp).

QUANTIFICATION AND STATISTICAL ANALYSIS

To quantify the number of GFP-FYVE, GFP-DFCP1, LC3 puncta and LD, a total of 30 cells were recorded and analyzed using the Axiovision automatic measurement program on the Zeiss LSM 510. These measurements were done on randomly-selected fields of view. Two-tailed unpaired Student's t test was performed for statistical analysis using GraphPad Prism software. All data are presented as mean ± SEM (***$p < 0.001$, **$p < 0.01$).